5-26-2017 12:00 AM

Full-Scale and Wind Tunnel Investigation of the Flow Field Over a Coastal Escarpment

Julien LoTufo, *The University of Western Ontario*

Abstract

A multiscale experimental approach, consisting of full-scale measurements and physical modeling in a laboratory environment, was conducted to investigate the flow field over a coastal escarpment on the Wind Energy Institute of Canada's research and development wind park. The influence of sea breeze inflow conditions, thermal stability and local topographic features on the flow field were examined.

The results of the full-scale study show that the near surface flow field is significantly influenced by the sea breeze circulatory coastal flow regime, creating larger shear layers with a smaller recirculation regions compared to cases of typical boundary layer flow.

Results of the physical modeling show an agreeable comparison between the hub height wind speeds at the location of a turbine was achieved under non-ABL conditions by simulating the non-ABL inflow. Additionally, significantly different mean and turbulent flow fields were observed for three different escarpment geometries.

Keywords

Co-Authorship Statement

Chapter Two will be submitted for publication under the co-authorship of Siddiqui, K., Hangan, H, Costache, A and Parvu, D. In this chapter, the full-scale experiments were conducted by Costache, A and Parvu, D. The lead author (LoTufo, J.) completed the data analysis, prepared the draft text and the final text after having it reviewed by the co-authors.

Chapter Three will be submitted for publication under the co-authorship of Hangan, H and Siddiqui, K. The lead author (LoTufo, J.) conducted the experiments and completed the data analysis, and the draft text before finalizing the text after review from the co-authors.

Acknowledgments

I would like to first and foremost thank my supervisor Dr. Kamran Siddiqui for his patience, guidance and support throughout my journey as well as my co-supervisor Dr. Horia Hangan for his wisdom and vision and shaping my research interests. I would like to thank them both for allowing me the opportunity to work within the WindEEE research group and to operate such unique tools.

A special thanks to Dr. Chowdhury Jubayer and Dr. Djordje Romaic for their insight into experimental and analysis techniques among various topics.

I would like to thank the WindEEE staff members Adrian Costache, Gerry Dafoe and Andrew Matthers who did everything they could to aid in the successful experimental outcome.

I want to thank Jubayer Chowdhury, Djordje Romanic, Dan Parvu, Mohammad Karami, Maryam Refan, Adrian Costache, Federico Canepa, Zeinab Sammani and Junayed Chowdhury for all the help and friendship I have received from them over the course of my experience.

Finally, I would like to thank my parents, Mertia and Lui, who did everything they could to encourage and support me throughout this experience.

Table of Contents

List of Tables

List of Figures

Chapter 1

1   Introduction

As an overwhelming amount of scientific evidence points toward human impact being the forefront of climate change, it is our responsibility to change our ways and provide a sustainable future for generations to come. Renewable energy, specifically generated by wind, has shown steady growth over the last few decades. Wind turbines continue to grow both in size and numbers while occupying greater areas both on and offshore. Not without some ecological footprint, wind turbines provide feasible source of clean energy and the continuing research and development in the wind energy industry is an essential piece of the solution to reducing the dependence on fossil fuels.

Global annual installed wind capacity has increased every year from 2000-2016 with the exception of 2013, while maintaining an average increase of 22% annually from 2007-2015 [1]. Additionally, wind has accounted for 3.7% of the global electrical production by the end of 2015 [2]. Growth in wind energy can be attributed to the increasing number of countries which support renewable energy policies. This growth attracted an increased number of investors which lead wind power to hold 38.6%, up 4% from 2014, of the total new investments in 2015 (excluding hydro greater than 50 MW) [2]. A larger influx of investments and incentives allows for further research and development into larger wind turbines, more reliable components, increased efficiency, better grid integration, and improved wind resource prediction.

For a wind farm developer, an accurate measure of the wind speed at a potential site is crucial to the determination of the power supplied by the project. A wind turbine's power output is given as [3]:

$$P = \frac{1}{2}\rho A U^3 C_p \eta \qquad (1.1)$$

where P is the power output, ρ is the density of air, U is the mean wind speed, A is the cross-sectional area, C_p is the power coefficient and η is the efficiency of the turbine. The power output is proportional to the cube of the mean wind speed and thus, small

inaccuracies in predicted on-site conditions can result is large discrepancies in the estimated power.

Flat sites, such as agricultural land, are often chosen for wind turbine placement as the flow characteristics are well understood. In the late 1970's the study of flow over complex terrain became a point of focus as there is often increased wind resources in these areas, and thus potential for wind energy. Complex terrain can be described as areas which have features such as steep ridges, hills, valleys, and forest canopies. The measurements and accuracy of on-site conditions in these areas become more difficult as effects induced by the terrain may create regions of separated flow and greater vertical velocities [4]. To improve the accuracy of both on-site measurements and predictive models a greater understanding of the interaction between complex terrain and atmospheric flow is necessary.

1.1 Atmospheric Boundary Layer

The atmospheric boundary layer (ABL) is the lowest portion of the atmosphere directly above the earth's surface which varies in depth between hundreds of meters to 1-2 kilometers. The first 10% of the ABL is the surface layer, or Prandtl layer, where the flow is not affected by the rotation of the earth and is influenced by friction from the surface and vertical changes in temperature [5]. The surface layer can be divided into the inertial sub-layer and the roughness sub-layer. In the inertial sub-layer, the velocity profile is considered to be logarithmic while close to the surface, in the roughness sub-layer, the flow is dependent on the individual roughness elements. At the surface, there is the classical no-slip condition where the velocity is equal to zero. The remaining upper 90% of the ABL is the Ekman Layer, where the pressure gradient and Coriolis force are not equal [6]. Topography plays an important role in the behavior of the ABL. Flat homogeneous terrain will, in conditions where there is no heating or cooling, provide a classical boundary layer. In complex terrain, the wind shear profile can be altered due the presence of hills which is illustrated in Figure 1. As the undisturbed wind approaches the crest of the hill, the flow accelerates upwind and experiences a speed up at the crest in the region closest to the hill, or the inner region, while the outer region remains unchanged by its presence. The ABL is often described by its thermal stability which effects the behavior of the boundary layer

velocity profiles as shown in Figure 2. The ABL is neutral when the potential temperature does not change with height and is often a result of shear driven flow due to increased wind speeds and cloud cover which adequately generate mechanical mixing and inhibits solar heating. The turbulent eddies present in a neutral flow are considered to be
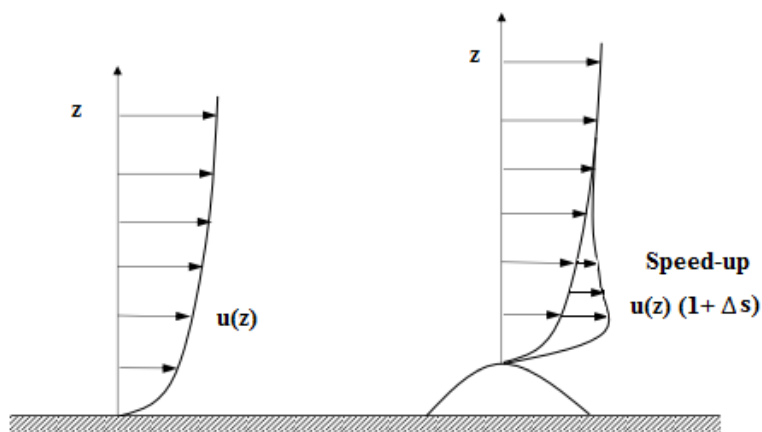
Figure 1-1: Illustration of the modified boundary layer due to speed-up over a hill adapted from Teunissen et al. [7].
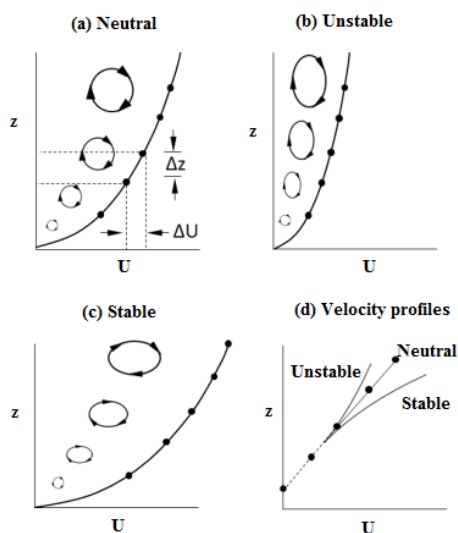
Figure 1-2: Effect of atmospheric stability on turbulent eddies and velocity profiles. Adapted from Oke [8]

roughly circular and increase in size with altitude [8]. Often, the thermal stratification in the ABL will not be neutral; it will be either stable or unstable. Stable stratification is present when there is a positive potential temperature gradient. Under these conditions, buoyancy forces are negative and vertical motions are suppressed, horizontally stretching eddies and resulting in a greater wind speed gradients. Unstable stratification, inversely, is present when there is a negative potential temperature gradient which encourages vertical motions with a positive buoyancy effect. Eddies in unstable ABL flows are stretched vertically and the wind speed gradient reduced due to the increased vertical motions that results in augmented mixing [8].

Quantifiable classification of the stability in the surface layer is commonly done using the Richardson number. The Richardson number is a ratio of buoyancy to shear in the role of turbulent production [5] and is given as:

$$Ri = \frac{\left(\frac{g}{\bar{\theta}}\right)\left(\frac{d\bar{\theta}}{dz}\right)}{\left(\frac{d\bar{u}}{dz}\right)^2} \tag{1.2}$$

where g is the gravitational acceleration, θ is the potential temperature, $d\bar{\theta}/dz$ is potential temperature gradient in the vertical direction and $d\bar{u}/dz$ is the wind speed gradient in the vertical direction. All the variables in the above equation are easily measurable which facilitate the calculation of thermal stability. A more widely recognized stability parameter is the ratio of height, z, to the appropriate eddy length scale called the Obukhov length [9]. The Obukhov length is defined as:

$$L = \frac{u_*^3}{k(\frac{g}{\theta_v})(\overline{w'\theta_{v'}})} \tag{1.3}$$

where θ_v is the virtual potential temperature which considers the humidity of the air and the static stability, $u_* = -(u'w')^{1/2}$ is the friction velocity, k is the von Karman constant equal to 0.41 and $\overline{w'\theta_v'}$ is the mean virtual potential temperature flux. This ratio of z/L is related to the Richardson number through the Monin-Obukhov similarity theory [5]. This similarity theory allows non-dimensional forms of atmospheric parameters such as wind shear and thermal stratification to be defined based on the scaling variables u_* and $T_* = $

$-(w'T')/u_*$. The integration of the non-dimensional wind shear parameter gives the equation for the logarithmic wind profile as:

$$u(z) = \frac{u_*}{k}\left(\ln\left(\frac{z}{z_o}\right) - \psi_m\right) \tag{1.4}$$

where, $u(z)$ is velocity at height z, z_o is the roughness length of the terrain and ψ_m is a function of z, z_o and z/L which accounts for stability. When ψ_m is equal to zero, the logarithmic profile becomes the standard profile for a neutral boundary layer, and like the Richardson number, stable conditions give a positive value of ψ_m and negative for unstable conditions.

1.2 Full-scale Measurements

Accurately measuring the wind conditions on a prospective wind turbine site is extremely important to the wind energy industry as these measurements not only used for determination of the economic feasibility of a project, but they are also used to establish wind turbine power curves. Once a wind developer has selected a site, the current practice is to instrument the site to determine the wind conditions for a period of one to three years [10] which is the used as an input for models to attempt a wind power prediction.

Generally, simple cup anemometers are used as they have been the industry standard for some decades to measure on site conditions. These simple mechanical systems are accurate when properly calibrated, cost effective and have sources of error that are well understood [11] making them a desirable tool. However, anemometer systems must be mounted on towers which add additional cost and can introduce new uncertainty into wind speed and direction measurements [12] with improper set up.

As wind turbines are becoming larger and more frequently placed in complex terrain, it becomes more difficult to accurately predict turbine power generation using measured wind conditions with the standard techniques. As only a few masts are used for on-site measurements [10], the measured characteristics at one point in space may not reflect the whole site due to changes in wind direction, wind speed and turbulence imparted by the topography. Moreover, the cost of towers, which increases roughly proportional to the

cubed height of the tower itself [13], is quickly becoming the downfall of mast based systems. It is becoming increasingly apparent that one measurement at hub height is not enough to fully characterize the flow behavior over the entire rotor diameter which can have significant impacts on potential energy predictions [14]. To combat these inherent issues of the growth of the industry, research into the use of remote sensing for wind energy applications has increased alongside the development of wind turbines.

1.2.1 Remote Sensing

Sound/Light Detection and Ranging (sodar/lidar) are two of the most commonly used remote sensing technologies. Sodars and lidars operate on the principle of the Doppler effect, detecting the frequency shift between the emitted sound or light source and the detected line-of-sight signal backscattered from temperature differences and moving aerosols in the atmosphere respectively [15]. A simple representation of a lidar system is shown in figure 3.
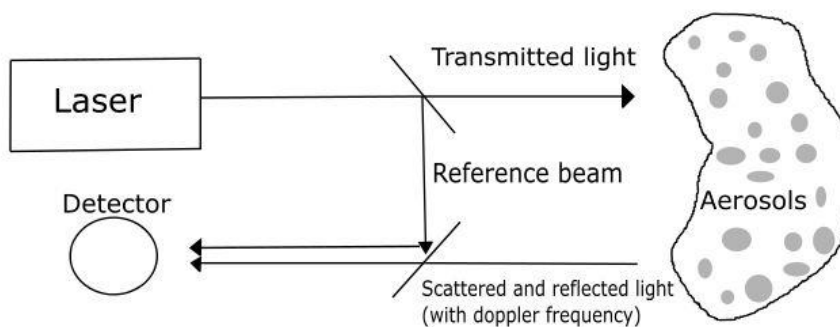
Figure 1-3: Depiction of a lidar system. Adapted from [13].

These instruments are only capable of measuring the wind component along the line of sight and use the relative angle of emitted source to infer a wind speed measurements and direction. The three-dimensional wind field can be measured using three instruments, but the setup becomes more complex. Both measurement techniques operate under the assumption of horizontal homogeneity as a volume of air is measured instead of a single point in space. This means the operation of these instruments relies on the assumption that the flow characteristics are the same throughout the entire sampling volume. At present,

these technologies are the most reasonable means of providing measurements at today's wind turbine heights and in complex terrain, however the accuracy of these measurement systems are still a subject of discussion. Comparison of measurements using remote sensing systems to the de facto standard cup anemometer is done to provide the wind energy industry confidence in these techniques.

Sodars have proven to be accurate in flat terrain, having shown good agreement (within 2%) to cup anemometer [16], but inherent issues related to the technique have limited their applications. Large measurement volumes at turbine hub heights and deterioration of measurement quality above wind speeds of 15 m/s, which is the nominal wind speed for larger wind turbines, are delaying the widespread use of sodars for wind resource assessment [17].

Lidars, on the other hand, have experienced significant growth in the industry, becoming widely used as they are inherently more accurate than sodars. Although there are two types of lidars, Continuous Wave (CW) and pulsed, each having their own characteristics, the subsequent discussion is focused on CW as it relates to this study. However, the general experimentation often includes both lidars and hence the conclusions are similar. In general, the optical source can be more precisely focused compared to sodars, as they use optical fibers with a 1.5μm wavelength source, so the backscatter off particles spreads less compared to the acoustic waves, leading to less noise [18]. Comparison of lidars to cup anemometers at have proven to provide accurate wind speed measurements in flat terrain [19, 20] as well as offshore [21, 22] with correlation coefficients close to 1 ($\geq$ 0.98) up to approximately 150 m.

Although proven in flat terrain, there is still some debate amongst the industry whether they are suitable for measurements in complex terrain. The general assumption of homogenous flow is no longer valid in homogenous terrain, thus causing a bias in the wind speed measurements. In recent years, the use of numerical modeling has helped calibrate lidars for complex sites which is highlighted by a comparative study by Pitter et al. [23]. Eight field campaigns around the world, each with complex terrain varying from low hills to mountains, resulted in biases of 1-2% to 11% respectively in the lidar measurements on

the site compared to nearby masts. Corrections involved employing either linearized models, such as WAsP, Computational Fluid Dynamics (CFD) using Reynolds-Averaged Navier-Stokes (RANS) or both. Using the deriving correction factors based on the information from these models, measurement errors were reduced to less than 2%, which is convincing evidence that the use of lidars for wind resource assessment, regardless of terrain, is bankable. For wind turbine micro-siting, the acceptance of remote sensing will result in wind speed measurement at realistic heights for use in Annual Energy Production (AEP) evaluations and allows for exploration of wind turbine sites which could not be assessed due to the constraints of the terrain and associated costs and complications of typical mast setups.

1.3 Wind Resource Assessment

1.3.1 Numerical Modelling

Once the full-scale measurements are taken, micro-scale models are often used to extrapolate the wind field from the location of measurements across the entire site to predict local wind conditions [10]. There are a few available microscale models which are acceptable today and have varying degrees of complexity and computing power. Linearized models, such as the previously mentioned WAsP are based on the equations formulated by Jackson and Hunt [24] which divide the flow into an outer layer where the flow is essentially inviscid and an inner layer where the shear stress is significant. These models require the least computing power and user input, making them a favorable choice among the industry. In recent years, the application of CFD using RANS has become more frequent throughout the industry, however it requires more computing power compared to linearized models. Large Eddy Simulation (LES) is the most complex and intensive of the numerical models. Although, as modern computing power continues to become more capable of matching its intensive requirements, LES may be more widely used [25, 26], but remains more of an academic tool at large.

The use of linearized models has proven to produce accurate wind characteristics in flat and homogenous terrain typical of a wind farm and over isolated low hills where the flow does not separate [27]. In more complex terrain, where changes in elevation can induce

high vertical velocities and separation thereby invalidating the linearized theory [4], these models have shown to be inaccurate. Developers often opt for the more advanced modeling techniques in these situations but have the tendency to be quite user dependent. Results of CFD models vary based on different boundary conditions and turbulence closure models chosen, leaving the user to apply the appropriate conditions based on their knowledge. The effect of user dependency is best depicted in the comparison of full-scale measurements over the Bolund peninsula to 57 different numerical and physical models [28] in which a wide range of speed-up ratios were found based on the same initial free-wind conditions. The cost restrictive wind farm development process may not be able to afford iterative models approaches as the computing cost increase of CFD is roughly 100 times more compared to linear models as estimated by Gasset et al. [27].

A few studies have aimed at quantifying the potential increase in AEP between linearized models and CFD to provide wind developers data to make an informed decision about whih tool to use in general scenarios. Ju et al. [29] compared the AEP of a 20 MW wind farm in complex terrain over the period of one year to the estimated values from a linearized and CFD models. It was concluded that although there was some deviation compared to the actual AEP for both models, the CFD compared better having a relative error of 2.5-3.5% versus 7.2-11.6%. from the linear model. Additionally, the results obtained using the linearized model varied based on the size of the domain used which did not affect the CFD results. It is difficult to draw conclusions from one case study as every site is different, but the advantages of CFD can be more clearly seen when considering the study done by Historov et al. [30]. In analyzing data obtained from 50 wind farm sites in both flat and complex terrain., an improvement of roughly 8% and 12% in the prediction of AEP was found when CFD models were used in flat terrain and complex terrain respectively.

The industry standard linearized models are often used outside of their domain to save time and cut costs during a wind farm development project. A better understanding of the local flow regime not just within a wind farm, but also within a specific turbine's rotor area along with adoption of more realistic models can help developers more accurately assess a project from its inception, reducing the initial risk. Higher AEP, reduced fatigue loading, and an

overall increase in turbine performance are just some of the incentives driving the continual research in this area.

1.3.2 Wind Tunnel Modelling

Topographic modeling in a wind tunnel has proved to be an effective tool to investigating the flow characteristics, specifically in cases of complex terrain, where the flow exhibits non-linear behavior. Validation of CFD models including new parameterizations are commonly done using data obtained from wind tunnel tests when full-scale data is not available.

There are several similarity laws that need to be followed for wind tunnel modeling to be considered an accurate representation of the atmospheric flow. From the conservation of momentum equations, the non-dimensional Rossby, Richardson and Reynolds numbers are the dynamic similarity parameters and from the conservation of energy equations, the Eckert and Prandtl number are the thermal similarities. In wind tunnel testing, it is highly unlikely that all of these similarity laws can be achieved so it is necessary to make simplifications [31]. The Rossby number cannot be satisfied in a wind tunnel which is non-rotational as it describes the effect of the Coriolis force on the flow compared to the inertial and centrifugal forces. Reasonable agreement between wind tunnel simulations and full-scale data have been found in complex terrain with distances between 10-20 km [32] and recommendations by Snyder [33] suggest that the modeled area should have a length less than 15 km. The Prandtl number, which compares the viscous diffusion and thermal diffusion rates, is satisfied as the medium used is air. The Eckert number is the ratio of kinetic energy to the difference in enthalpy over the boundary layer and is satisfied in neutral conditions. The Richardson number is directly related to the stability of the atmosphere and is the ratio of buoyancy to shear. The similarity of the Richardson number is an interesting topic, and one that forms part of the motivation for this research, as full-scale flows which are observed are often depart from neutral conditions and hence are not reproducible in a typical wind tunnel. Lastly, the Reynolds number is almost impossible to fully match, although it is assumed that above a threshold the flow behavior becomes independent.

Through these assumptions and proper geometrical scaling, wind tunnels can be a very useful tool for assessing wind over complex terrain. Studies conducted range from forest canopies, hills with simple sinusoid shapes and escarpments of varying slopes to mountains. As hills and escarpments are more related to the present study, these will be focused on with some detail. Bowen and Lindley [34] examined the effects of 1:300 scale, sharped edged escarpments with varying slopes from 1:1 to 4:1 on the near surface mean and turbulent flow characteristics. The modifications to the mean flow, via speed-up factor, were confined to three escarpment heights above the feature and ten escarpment heights downstream and the slope only had a small effect on the mean flow. The turbulence intensity increased downstream of the crest with increasing slope. Ngo and Letchford [35] modelled escarpments and symmetrical ridges at a 1:1000 scale, focusing on the effects of surrounding surface roughness and slope angle of the feature. The speed-up factor near the crest and the extent to which the downstream areas were affected are considered for design of structures, comparing the results to various international codes, as well as wind energy potential. Through comparing multiple geometries to multiple standards, the consensus was that the wind load codes were not conservative in defining the spatial extent of the influenced region downstream. Ishihara et al. [36] studied the mean and turbulent flow behavior of flow over three dimensional steep hills with a focus on the turbulence characteristics of the near-wake downstream. Ferreira et al. [37] examined the flow characteristics over two dimensional hills of sinusoidal shape and found that steeper hills caused much larger recirculation zones compared to shallow hills directly affecting the feasibility of linearized models.

There have been several studies regarding reproducing full-scale measurements on scaled models of real topography. Perhaps the most notable of these experiments are the Askervein hill experiments conducted by Teunssian et al. [7] and the Kettles hill experiment by Salmon et al. [38] which are the benchmark field experiments for physical and numerical model validation. Three scaled models of the Askervein hill were used to conduct wind tunnel testing and the results proved to be in close agreement with the full-scale measurements. There was, however, some error on the leeside where separation occurred. In the Kettles hill experiment it was noted that small deviations in the incident wind direction caused deviation from full-scale results due to changes in the upwind slope.

These experiments are good examples of the ability of wind tunnels to accurately predict full-scale measurements of flow over low hills. McAuliffe et al. [39] conducted experiments of flow over a 1:1500 scale models of a coastal wind farm in Gros-Morne, Quebec, Canada. A good comparison was made between full-scale data, showing deviations of no more than 10% although the wind shear profile was not adequately matched, with the full-scale data having greater shear.

1.4 Motivations and Objectives

The wind industry standard linearized models are appropriate for wind resource assessment in flat or gentle sloping terrain, but have shown to be less accurate in complex terrain compared to advanced modelling techniques. The use of various CFD codes have shown variability in the results depending on user input and thus necessitates a better understanding of the complex flow regimes in complex terrain, especially in situations where flow separation and reattachment are present.

Field measurements are the most useful means of obtaining insight into the real physical processes of the flow to further improve current modeling techniques. There are instances of field campaigns, such as the Bolund campaign [40], which used a plethora of instruments to provide a more detailed analysis for modelers, but these often require large amounts of resources. However, for the most part, limitations of time, cost and uncertainty allow for only a few locations to be probed with only a few instruments. This limits the ability to accurately assess a site's potential and provide a comprehensive database for model validation. Remote sensing has proven to be accurate in flat terrain, and relatively accurate in complex terrain with some corrections, allowing for an easier setup and more control over the measurement locations. Recently, at the Technical University of Denmark (DTU), development of a customized commercial lidar which allows for programmable scanning patterns and smaller probed air volumes. Successful implementation of this lidar has been shown on a few accounts, including investigating the wake region behind the Bolund escarpment [41], leading to the eventual use of this instrument in this study. Using lidars to measure wind speed not only offers a more complete picture in complex terrain, but also more accurate wind speed evaluations over the entire rotor diameter of a wind turbine from the ground. Furthermore, they may be mounted on a wind turbine nacelle to more

accurately measure turbine level upstream wind speeds and correct yaw alignment, which can lead to increased overall AEP [13].

Within the research community, the wind resource assessment methods that are most often used are limited by the similarity laws of classical wind tunnels to neutrally stable flows. Herein lies a limitation, as real atmospheric flows are often non-neutral. This has put a constraints on the conditions in which potential wind farm sites can be evaluated through these models. It is possible for CFD models to include thermal effects but this further increases the complexity of a method which has not proven to be fully dependable. When accurately representing the ABL by considering thermal effects in CFD modelling, a significant improvement is AEP estimation is possible [30] providing further incentive in this field. The performance of wind turbines, including AEP, can be directly affected by the stability effects of the atmosphere due to modifications of wind shear profiles over the rotor area and turbulence characteristics [42]. As coastal areas are advantageous for their wind resources, it is important to have an increased understanding of the effects of variable wind climates due to temperature difference and roughness changes between the surfaces [43] and their interaction with complex terrain, which is often found in these areas.

1.4.1 Objectives

The main objective of this study was to investigate the flow field over a complex topography by adapting a multi-scale approach using both:

- Full-scale measurements

- Scaled modeling in laboratory environment

To complete the first objective, full-scale measurements were conducted on the Wind Energy Institute of Canada's Research and development wind park near a coastal escarpment. This coastal topography can be characterized as a sharp-edged, steep escarpment with a long upstream open-water fetch, which makes it desirable from a modelling standpoint. The wind speed was measuring using a scanning lidar and the data was analyzed in the form of velocity and turbulence intensity profiles based on changes to the upstream conditions and thermal stability during the measurement period.

The second research objective was fulfilled through physical modelling of the full-scale measurement site. The WindEEE dome allows for testing of large scale models as well as a wide range of inflow conditions. Three different escarpment geometries, seen from three different wind directions, were investigated to determine the influence of the topography on the flow field under two different inflow conditions. Full-scale inflow profiles were physically simulated, which differed from the classical boundary layer flow by manipulating individual and comparison of velocity profiles to full-scale measurements was done.

The significance of the inflow conditions, thermal stability and local topographic features on the flow behaviour over topography are highlighted in this work, contributing to the broader research by means of further improving both numerical and physical modelling.

1.5   Organization of Thesis

This thesis is written in the integrated article format as specified by the Faculty of Graduate Studies at Western University.

Chapter 1 contains the relevant background information on the challenges and current trends of the wind energy industry in terms characterizing flow over complex terrain focused on the purpose of wind resource assessment and wind turbine siting.

Chapter 2 investigates the effect of the upstream conditions and thermal stability on the near surface flow field downstream of the escarpment edge. A scanning lidar is used to measure velocity and turbulence intensity profiles and the properties of the wake are characterized up to 15 m. Additionally, the effect of inflow conditions Chapter 2 is to be submitted to a boundary layer meteorology journal.

Chapter 3 consists of the physical simulation of the coastal full-scale measured inflow and its influence on the flow field compared to a typical boundary layer flow from three wind directions, each with different complex local topography. Measurements were conducted by means of Cobra Probes at multiple positions downstream of the leading edge and data is presented in the form of mean velocity and turbulent statistics. The importance of proper inflow conditions and effects of local topography are highlighted in

this chapter. Chapter 3 forms the basis of a paper to be submitted to a wind energy journal.

Chapter 4 includes the conclusions and suggestions for future work in this area of research.

References

[1] Global Wind Energy Council, 2017. Global wind statistics 2016.

[2] REN21, 2016. Renewables 2016 global status report

[3] Manwell, J.F., McGowan J.G., and Rogers A.L., 2009. Wind energy explained, theory design and application. 2nd Ed, John Wiley & Sons Ltd. United Kingdom.

[4] Palma, J. M. L. M., Castro, F.A., Ribeiro, L.F., Rodrigues, A.H., and Pinto, A.P., 2008. Linear and nonlinear models in wind resource assessment and wind turbine micro-siting in complex terrain. Journal of Wind Engineering and Industrial Aerodynamics, 96, 2308–2326

[5] Kaimal, J. C., and Finnigan, J.J., 1994. Atmospheric Boundary Layer Flows: Their Structure and Measurement. New York, Oxford UP

[6] Cushman-Roisin, B., and Beckers, J.M., 2007. Introduction to Geophysical Fluid Dynamics, 2nd Ed, Academic Press.

[7] Teunissen, H.W., Shokr M.E., Bowen, A.J., Wood, C.J. and Green, D.W.R., 1987. The Askervein hill project: wind tunnel simulations at three length scales. Boundary Layer Meteorology, 40, 1–29.

[8] Oke, T.R., 1987. Boundary-layer climates. 2nd edition, Taylor and Francis Group. New York.

[9] Emeis, S., 2014. Wind Energy Meteorology: Atmospheric Physics for Wind Power Generation. Springer

[10] Rodrigo, R., 2010. State-of-the-art of wind resource assessment, CENER National Renewable Energy Centre

[11] Kristensen, L., 1998. Cup Anemometer Behavior in Turbulent Environments. Journal of Atmospheric and Oceanic Technology, 15, 5-17.

[12] Petersen, E. L., Mortensen, N.G., Landberg, L., Højstrup, J., Frank, H.P., 1998. Wind Power Meteorology. Part II: Siting and Models. Wind Energy, 1, 55-72

[13] Peña, A., Hasager, C.B., Badger, M., Barthelmie, R.J., Bingöl, F., Cariou, J-P., Emeis, S., Frandsen, S.T., Harris, M., Karagali, I., Larsen, S.E., Mann, J., Mikkelsen, T., Pitter, M., Pryor, S., Sathe, A., Schlipf, D., Slinger, C., Wagner, R., 2015. Remote Sensing for Wind Energy. DTU Wind Energy. 260 p. (DTU Wind Energy E; No. 0084(EN)).

 [14] Wagner, R., I. Antoniou, S. M. Pedersen, M. S. Courtney, and H. E. Jørgensen, 2009: The influence of the wind speed profile on wind turbine performance measurements. Wind Energy, 12, 348–362.

[15] Emeis, S., 2011. Surface based remote sensing of the atmospheric boundary layer. Springer, New York.

[16] National Renewable Energy Laboratory (NREL). Comparison of Second Wind Triton Data with Meteorological Tower Measurements; Report TP47429; NREL: Golden, CO, USA, 2010.

[17] Hansen, K. S., 2006. Validation of Sodar Measurements for Wind Power. In EWEC2006: Scientific Proceedings European Wind Energy Association (EWEA).

[18] Courtney, M., Wagner, R., Lindelöw, P., 2008. Testing and Comparison of lidars for profile and turbulence measurement in wind energy. IOP Conference Series: Earth and Environmental Science 2008. 1:012021.

[19] Antoniou, I., Ejsing Jørgensen, H., Mikkelsen, T., Friis Pedersen, T., Warmbier, G., & Smith, D., 2004. Comparison of wind speed and power curve measurements using a cup anemometer, a LIDAR and a SODAR. In Scientific proceedings (pp. 47-51). London: European Wind Energy Association (EWEA).

[20] Smith, D.A., M. Harris, A.S. Coffey, 2006: Wind Lidar Evaluation at the Danish Wind Test Site in Høvsøre. –Wind Energy **9**, 87–93.

[21] Kindler, D.; Oldroyd, A.; MacAskill, A.; Finch, D. An eight month test campaign of the Qinetiq ZephIR system: Preliminary results. Meteorologische Zeitschrift, 2007, 16, 479-489.

[22] Peña, A., Hasager. C.B., Gryning, S., Courtney, M., Antoniou, I., and Mikkelsen, T.,2009. Offshore Wind Profiling Using Light Detection and Ranging Measurements. Wind Energy 12, 105-24.

[23] Pitter, M., Abiven, C., Vogstad, K., Harris, M., Barker, W., Brady, O., 2012. Lidar and computational fluid dynamics for resource assessment in complex terrain. In: Proceedings of the European Wind Energy Association Conference and Exhibition. Copenhagen, Denmark, p. 10.

[24] Jackson, P. S. and Hunt, J. C. R., 1975. Turbulent flow over a low hill, Quart. J. Roy. Meteorol. Soc. 101: 929–955

[25] Ayotte, K.W., 2008. Computational modelling for wind energy assessment. Journal of Wind Engineering and Industrial Aerodynamics 96, 1571–1590.

[26] Ayotte K.W., Sullivan P.P., and Patton E.G., 2010. LES and wind tunnel modelling over hills varying steepness and roughness. Fifth International Symposium on Computational Wind Engineering (CWE2010), 23-27 May, Chapel Hill, North Carolina, USA

[27] Gasset, N., Landry, M., and Gagnon, Y., 2012. A comparison of wind flow models for wind resource assessment in wind energy applications. Energies, 5, 4288–4322.

[28] Bechmann A., Sørensen, N.N., Berg J., Mann J., and Réthoré, P.-E., 2011. The Bolund experiment, Part II: blind comparison of microscale flow models. Boundary-Layer Meteorology, 141, 245–271

[29] Ju, B., Jeong, J., Ko, K., 2016. Assessment of Wind Atlas Analysis and Application Program and Computational Fluid Dynamics Estimates for Power Production on a Jeju Island Wind Farm. Wind Engineering 40, 59-68. DOI: 10.1177/0309524X15624346

[30] Hristov, Y., Oxley G., and Žagar, M., 2014. Improvement of AEP predictions using diurnal CFD modelling with site-specific stability weightings provided from mesoscale simulation, TORQUE 2014, Journal of physics conference series: 524

[31] Conan, B., Chaudhari A., Aubrun S., van Beeck J., Hämäläinen, J., and Hellsten A., 2015. Experimental and Numerical Modelling of Flow over Complex Terrain: The Bolund Hill. Boundary-Layer Meteorol. 158, 183–208.

[32] Meroney, R.N, 1990. Fluid Dynamics of Flow over Hills/Mountains - Insights Obtained through Physical Modeling. Atmospheric Processes over Complex Terrain. 145-171.

[33] Snyder W, 1981. Guidelines for fluid modelling of atmospheric diffusion. EPA Office of Air Quality, Planning and Standards, Research Triangle Park, USA. Tech. rep., EPA-600/8-81-009

[34] Bowen, A. J., and Lindley, D., 1977. A Wind-tunnel Investigation of the Wind Speed and Turbulence Characteristics Close to the Ground over Various Escarpment Shapes. Boundary-Layer Meteorology 12.3:259-71

[35] T. T. Ngo and Letchford, C. W., 2009. Experimental Study of Topographic Effects on Gust Wind Speed. J. Wind Eng. Ind. Aerodyn. 97, 426-438.

[36] Ishihara, T., Hibi, K., Oikawa, S., 1999. A wind tunnel study of turbulent flow over a three-dimensional steep hill. Journal of Wind Engineering and Industrial Aerodynamics 83, 95–107.

[37] Ferreira, A.D., Lopes, A.M.G., Viegas, D.X., Sousa, A.C.M., 1995. Experimental and numerical simulation of flow around two-dimensional hills. Journal of Wind Engineering and Industrial Aerodynamics 54/55, 173–181.

[38] Salmon, J. R., Teunissen, H. W., Mickle, R. E., Taylor, P. A., 1988. The Kettles Hill Project: Field Observations, Wind-tunnel Simulations and Numerical Model Predictions for Flow over a Low Hill. Boundary-Layer Meteorology 43, 309-343

[39] McAuliffe B.R., Larose G.L., 2012. Reynolds-number and surface-modeling sensitivities for experimental simulation of flow over complex topography. Journal of Wind Engineering and Industrial Aerodynamics 104–106, 603–613.

[40] Berg, J., Mann, J., Bechmann, A., Courtney, M. S., Jørgensen, H. E., 2011. The Bolund Experiment, Part I: Flow Over a Steep, Three-Dimensional Hill. Boundary-Layer Meteorology, 141, 219-43.

[41] Lange, J., Mann, J., Angelou, N., Berg, J., Sjöholm, M., Mikkelsen, T., 2015. Variations of the Wake Height over the Bolund Escarpment Measured by a Scanning Lidar. Boundary-Layer Meteorology 159, 147-159.

[42] St. Martin, C. M., Lundquist, J.K., Clifton, A., Poulos, G. S., and Schreck, S. J., 2016. Wind Turbine Power Production and Annual Energy Production Depend on Atmospheric Stability and Turbulence. Wind Energy Science, 1, 221-236

[43] Barthelmie, R. J., 1999. The Effects of Atmospheric Stability on Coastal Wind Climates. Meteorological Applications 6, 39-47.

Chapter 2

2 Field Investigation of Inflow and Atmospheric Stability Effects on Flow Over an Escarpment

2.1 Introduction

Atmospheric Boundary Layer (ABL) flows over homogenous terrain are well understood from a fluid dynamical perspective and are typical sites for wind farms. Industry standard linearized models provide wind developers with accurate estimates of wind characteristics in these regions [1]. However, for wind farm designing in complex terrains, the same models provide less accurate results [2]. This is attributed to the limitations of linearized models to properly capture the underlying flow behavior emerged due to the presence of complex topographic geometry. New developments in computing power have allowed the emergence of more complex numerical models, that can simulate the flow behavior in complex geometries but the degree of accuracy too often depends on user input [3]. One inherent deficiency in the computational approach is the lack of advanced understanding of flow dynamics in complex topographic regions, which is vital for model improvements. Complex terrain, which is characterized by large, abrupt changes in surface characteristics such as elevation or roughness, can significantly affect both the mean and turbulent characteristics of the local flow field. Specifically, flow over steep hills or escarpments can generate complex spatial-temporal structures such as flow separation and shedding vortices [4, 5]. Although often advantageous from a wind energy potential standpoint, the highly turbulent wakes generated in such terrains can induce increased stresses and fatigue on the turbine blades and structure [6].

Over the last four decades, researchers have conducted many full-scale field studies of flow over hills and escarpments, most of which have been accompanied by wind-tunnel tests and/or computational modelling. The most notable of these full-scale campaigns is Askervein hill which provided an extensive study of neutral ABL flow over a hill in Scotland [7,8]. Upstream, hilltop and downstream vertical profiles of mean wind speed and turbulence were measured showing wind speeds at the hilltop increasing by up to 30% with a weak, intermittent separation region at the leeside. Turbulence intensities and wind

speeds at the top of the hill showed significant variability with wind direction. The internal boundary layer growth and the influence of roughness variations are also described in this study. The data from that campaign have been used to validate simplified linear models, RANS and LES [9, 10] as well as wind tunnel models [11]. Other notable full-scale campaigns include Black Mountain (Canberra, Australia) [12], Kettles Hill (Alberta, Canada) [13] and Nyland Hill (Somerset, United Kingdom) [14]. The effects of changes in roughness as well as the influence of coastal topography on vertical wind speed profile were investigated in the Risø peninsula over a 10-m escarpment [15]. Internal boundary layer thickness and speed up ratio were approximated well using the analytical approach from Jackson and Hunt [16] despite the difference in topography. More comprehensive studies over escarpments were conducted by Bowen [17] in New Zealand and Emeis et al. [5] in Denmark. Bowen [17] measured vertical wind speed and turbulence profiles over sloping and steep coastal escarpments. Much larger speed-ups and increase in longitudinal and lateral turbulence intensities were seen in the case of the steep escarpment along with a wake with a height equal to the escarpment height at four times the escarpment height downstream. The Hjardemål experiment [5] consisted of measurements with stable, neutral and unstable ABL flows. The stable flow proved to have the greatest speed up at the crest of the escarpment which persisted further downstream than the other two cases. Formation of an internal boundary layer was evident due to the step change in surface profile from sea to land. A wind tunnel test of similar escarpment geometry [18] overestimated the extent of the accelerated flow regions but the streamwise turbulence intensity agreed well with that from the field. A numerical study which used a model based on second-order turbulence closure [19], predicted friction velocity and streamwise turbulence intensity with close agreement.

Much of the research previously mentioned was focused on flow over low hills with a slope of roughly 20°. In these cases, most of the topography being investigated were well inland and free from sea-land interfaces. Hence, these studies were primarily concerned with the mean horizontal velocity profiles and turbulence intensity in neutral atmospheric conditions and less with the influence of topography on the modification of turbulent structures or non-ABL inflow profiles. More recently, a series of extensive field campaigns conducted at the Bolund hill in Denmark [20], a 12-m tall sharp escarpment, set out to

provide yet another benchmark experiment which allows for validation of numerical models. The first campaign consisted of measurements along two transects by erection of many meteorological masts. Flow separation on the leeside of the escarpment was seen accompanied by transient wake behavior which has a height that is directional dependent. Wind speed increments of up to 30% were seen along particular wind directions with an enhancement in turbulence intensity by up to 300% at the top. The measurements during this campaign were conducted under majority slightly stable and neutral wind conditions, while the data was presented as neutral. This was done as there was little variability due to stability compared to compared to the impact of the flow from the topography. The second campaign sought out to better investigate the transient wake using a scanning lidar [21, 22]. Vertical velocity profiles and turbulence intensity were measured up to a height of 7 m showing reverse flow near the surface and a wake height dependence with wind direction was clearly defined.

The present study is concerned with the characterization of the upstream wind shear profile to a local wind turbine and investigating the impact of these conditions on the near surface flow field over a coastal escarpment. An increased number of wind turbines are being installed inland in coastal regions to take advantage of the long, open water fetches and relatively high wind speeds [23]. The local flow regime in these areas are modified by complex sea-land topography, such as escarpments, and thermally-driven flows. Differential heating of the land and sea surfaces causes cooler stable air to flow over the warm land creating circulatory sea-breeze flow systems with gust type characteristics [24]. These atypical flow conditions pose yet another challenge to the common predictive models, which already struggle in complex terrain, as they assume neutral atmospheric conditions where temperature gradients do not affect the wind shear profile [25, 26]. Therefore, it is of utmost importance to provide a better understanding of the not just the flow characteristics over these types of terrain, but also the flow behavior under non-ABL conditions. An increased knowledge of the mean flow and turbulent characteristics from fluid dynamical perspective under these conditions will allow for improvements on the wind resource assessment in these areas as well as the performance and wind loading on turbines.

2.2 Windscanner and Data Processing

The windscanner is a short-range coherent wave Light Detection and Ranging (LiDAR) device developed by the Wind Energy Department at the Danish Technical University (DTU). Essentially a modified ZephIR 150 lidar, this instrument can take line-of-sight wind speed measurements at distances between 10 m – 200 m with high spatial and temporal resolutions. The line-of-sight wind speed is measured by taking an average of the Doppler-shifted backscatter within the focal volume from aerosols such as dust or moisture in the atmosphere [27] and is based on the principles described in Karlsson et al. [28]. The windscanner has a patented scanning head with two individually controlled prisms for increased agility of the light beam [29]. Each prism within the head can deflect the beam by ±30° and through the rotation of two prisms simultaneously, rapid steering and synchronization of the beam's focal location is possible within a ±60° cone. Additionally, the scanning head is equipped with an acousto-optic modulator (AOM) which provides the ability to measure the sign of the Doppler shift, either towards or away from the instrument. The control system records the position of each individual prism to determine the direction of the focal volume line-of-sight. A full, detailed description of the methodology of the windscanner can be found in Sjöholm et al. [30].

The windscanner's adjustable focus point has a distance specific probe length defined as the width of the intensity profile along the directed line-of-sight, which has a maximum intensity at the center of the probe. The probe intensity profile follows a Lorentzian distribution [31] which varies roughly quadratically with the distance from the windscanner. The probe length, referred to as the Full Width Half Maximum (FWHM) is shown in Figure 2-1. These theoretical probe lengths are calculated based on the characteristics of the optical components as well as experimental testing by its manufacturer.

In the present study, a line-of-sight wind speed sampling rate of 250 Hz was used, with each measurement consisting of the instantaneous average of 500 Doppler spectra in real time. Before processing the raw Doppler spectra, averaging is done to reduce the effective background noise. This is followed by the thresholding and subsequent analysis of the spectral peaks to determine the wind signal. A more detailed description of the data

processing can be found in Angelou et al. [32]. The capabilities of the windscanner allow for measurements of wind speeds from
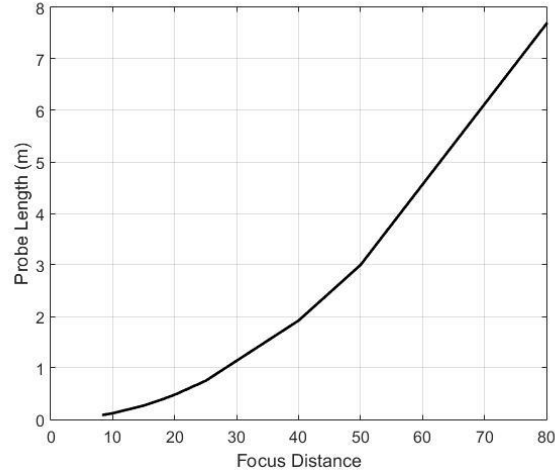
Figure 2-1: Values of FWHM at multiple distances from the windscanner

0.18 m/s up to roughly 47 m/s along the line-of-sight. Wind speeds close to zero [33] and near the surface are the limiting factors while using the windscanner. Cases of zero velocity may also occur when the flow is perpendicular to the line-of-sight.

The use of only one windscanner in the present experiment limits the ability to resolve the two or three-dimensional flow field. However, information about the horizontal flow field can be inferred from the line-of-sight wind speed with a beam inclination angle. An estimate of the horizontal wind speed based on the beam inclination is given as:

$$v_h = \frac{v_{los}}{cos\theta} \tag{2.1}$$

where θ is the angle of the beam relative to the horizontal and v_h is the horizontal wind speed. Hence, when the beam is at a given angle relative to the direction of the flow, the measured line-of-sight wind speed is a percentage of the actual wind speed. The inclination of the beam at each measurement point is calculated using the focal distance and the height of the focal location.

Calibration of the windscanner through a hard target test was conducted using a rotating wheel with a diameter of $D = 0.19$ m (7.58 inches) and angular velocity of $\omega = 351.86$ rad/s (3360 rpm). These quantities were measured using a caliper and tachometer which have uncertainties of ±0.01 mm and ±0.05%, respectively. The expected linear velocity of the reference disk was calculated using the radius and the angular velocity, which was $v = 33.87$ m/s tangential to the surface. The windscanner measured a velocity of 33.91 m/s which is within minimum measurable interval of ±0.18m/s. Moreover, this exercise, to some degree, proves the validity of the data processing algorithm. The accuracy of the flow velocities measured by the windscanner, was assessed by their comparison with those measured by Cobra Probes at the Wind Engineering, Energy and Environment (WindEEE) dome.

The WindEEE Dome is the world's first three-dimensional wind chamber with the ability to simulate synoptic and non-synoptic wind flows at large scales. The test chamber is a hexagon of 25 m in diameter which contains 106 fans individually controlled fans and operates in either a closed or open circuit return mode. Each fan has a diameter of 0.8 m and can be individually controlled through variable frequency drives to achieve a maximum velocity of approximately 25 m/s at a nominal power of 30 kW. Additionally, variable height roughness elements inside the chamber allow for a large range of atmospheric boundary layer flows to be simulated. A full description of the test facility can be found in Hangan [34], while a depiction of the chamber is shown in Figure 2-2.
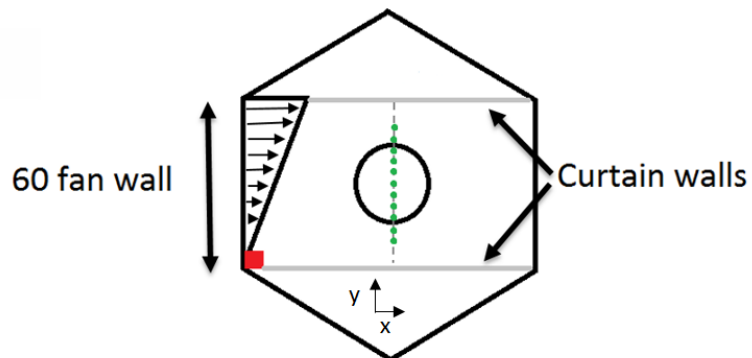
Figure 2-2: Schematic of test setup. Red square is the position of the windscanner and green circles are Cobra Probes.

In the calibration test, the 60-fan wall (X = 0 m) was used to physically simulate horizontally sheared flow across the center of the chamber (X = 12.5 m) without any roughness elements being used. In this scenario, the dome acted as a quasi-closed-circuit wind tunnel by deploying curtain walls which dropped down from the ceiling and fastened to the floor. The curtain walls span the inner 15 m of the chamber, covering the length of the 60-fan wall and formed a rectangular cross-section as seen in figure 2-2. A horizontal rake of 11 Cobra Probes, which are four-holed pressure probes capable of measuring the three components of velocity, was placed across the chamber with each probe positioned at the center of the inner 11 columns of fans. Each Cobra Probe in the horizontal rake was positioned 1.3 m from the floor, aligning them with the scanning head of the windscanner in its 90° position as shown on the right in Figure 2-3. The windscanner was
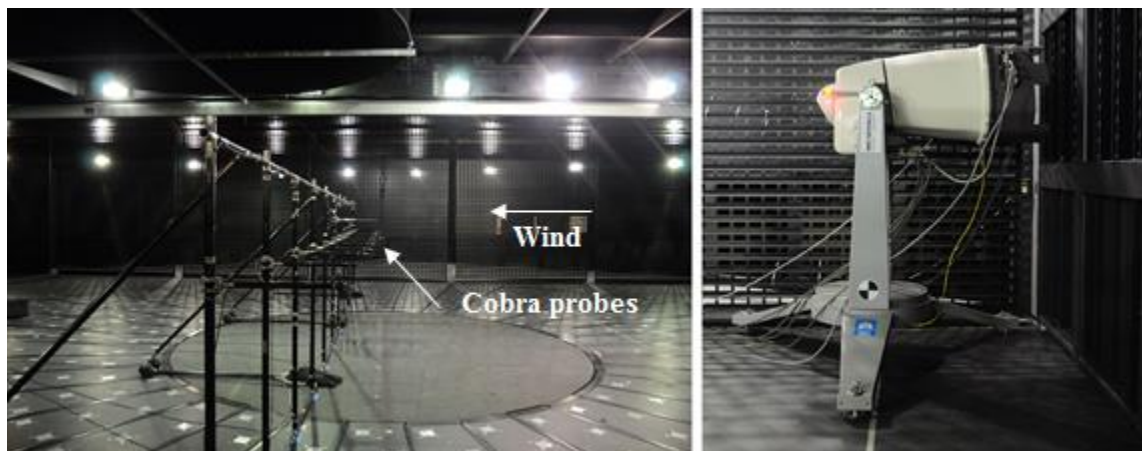
**Figure 2-3: Cobra Probe array at the center of the chamber (X = 12.5) (left).
Orientation of the windscanner in front of the first column of fans (right).**

placed in the center of the first column (Y = 0) of fans located at the bottom of the 60-fan wall as shown in figure 2-2. Hence, the first column of fans was not operated during this experiment. The Cobra Probes sampled at 10,000 Hz with an output rate of 1250 Hz for 4 minutes while the windscanner simultaneously sampled at 250 Hz, scanning across the chamber 5 cm below array of probes. This scanning configuration was considered optimal to minimize the inherent interference with the surroundings during measurements. In the subsequent data analysis, the Cobra Probes were down sampled to match the 250 Hz sample rate of the windscanner. Evident peaks in the spectra as a result of interference with

the side curtain walls and the rake setup were filtered prior to post processing. Three configurations of the fans were used to produce horizontally sheared flow with three different gradients of varying magnitudes. The mean streamwise velocity (U) component as measured by the Cobra Probes and the corrected line-of-sight wind speed component measured by the windscanner across the length of the chamber are plotted in Figure 2-4 for comparison. It is evident from the plot that there is a very good
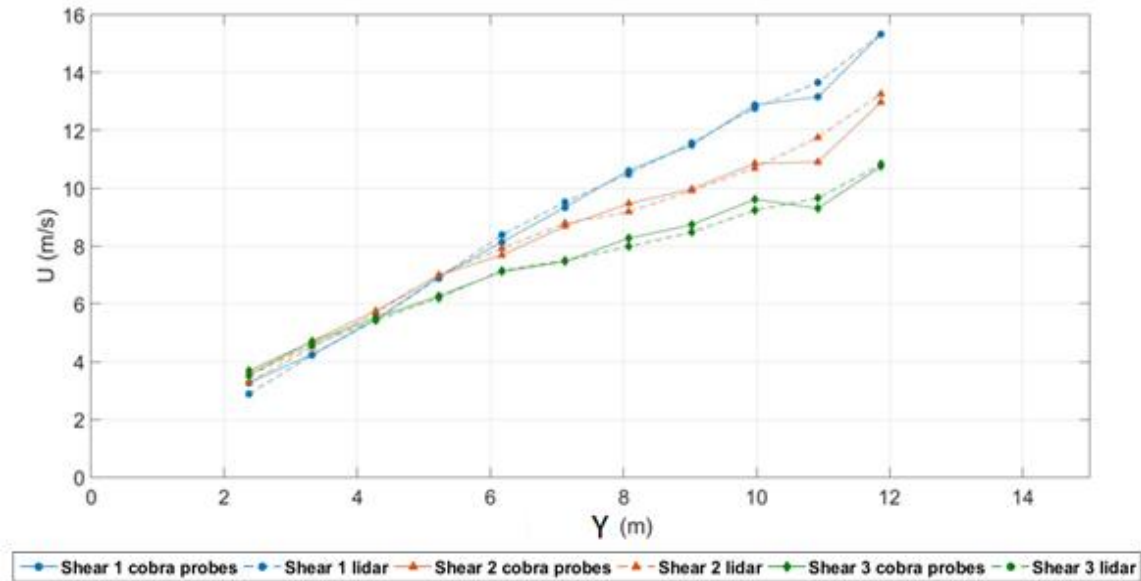
Figure 2-4: Horizontal shear profiles spanning the center of the chamber.

agreement between the corrected line-of-sight velocity measured by the windscanner and the streamwise component measured by the Cobra Probes. The difference in the Cobra Probe and windscanner velocities was within 8% confirming that the windscanner and its processing algorithm accurately computes the flow velocity. The largest differences were found in the low speed region near the first column possibly due to filtering of the high noise levels which contain low amplitude frequencies due to wind. At $Y = 11.4$ m from the first column of fans, there are also large differences between the two measurement techniques but considering the agreement at every other position and the fact that this trend is consistent through all three configurations, it is reasonable to assume that this difference is caused by some measurement uncertainty in the Cobra Probe or the data acquisition cable at that location. A previous study has shown that winds canners can provide accurate and

useful measurements inside wind tunnels, comparable to typical point measurement techniques [35], which is confirmed by the present study. Moreover, the results of this calibration provide confidence in the line-of-sight correction assuming the flow direction is known.

2.3 Prince Edward Island Wind Energy Experiment (PEIWEE)

2.3.1 Campaign and Site Description

In May 2015, a full-scale campaign was set out at the windfarm of the Wind Energy Institute of Canada (WEICan) located at the Research and Development park in North Cape, Prince Edward Island, shown in Figure 2-5. The objectives of this campaign were to study the impact of complex topography and wake effects on turbine performance. The surrounding area is comprised of long stretches of flat open terrain bounded by a coastal escarpment which has an upstream open water fetch >55 km to the west. Forested areas are also located to the East and South. The research park houses five 2MW, 80 m tall wind turbines with rotor diameters of 93 m. Four out of five turbines (depicted as T1-T4 in Figure 2-5) are located parallel with the coastline which varies in height from 6 m near T1 to 14 m near T4. A series of masts and lidars were also deployed during the study to investigate near surface parameters downstream of the escarpment by Barthelmie et al. [36]. The windscanner was used to measured turbine inflow over the coastal escarpment and a forest canopy near turbine 4 as well as inflow to turbine 3 which is affected by wakes from T4 and T2 depending on the wind direction. The present study focuses on measurements taken on May 15, 2015 of the sea breeze inflow to turbine 4 over the escarpment of which an image and contour plot is shown in Figure 2-6. The measurement location is denoted by red markers in Figures 2-5 and 2-6.

During the experiment, WEICan provided 10-minute mean wind speed, wind direction, atmospheric pressure, and temperature data acquired from the IEC compliant 80 m mast located about 500 m from the coastline shown in Figure 2-5. Additionally, turbine 4 provided 10-minute mean data of wind speed, nacelle position and active power. In the afternoon of May 15th, the windscanner was placed at two locations downstream of the

escarpment near T4 as shown by red markers in Figure 2-5. The second location was displaced downstream by 5 m from the first at 47° 1.998' N, 64° 1.186' W and 47° 2.0' N, 64° 1.180' W, respectively. Measurements were made between 12:30 pm to1:40 pm AST
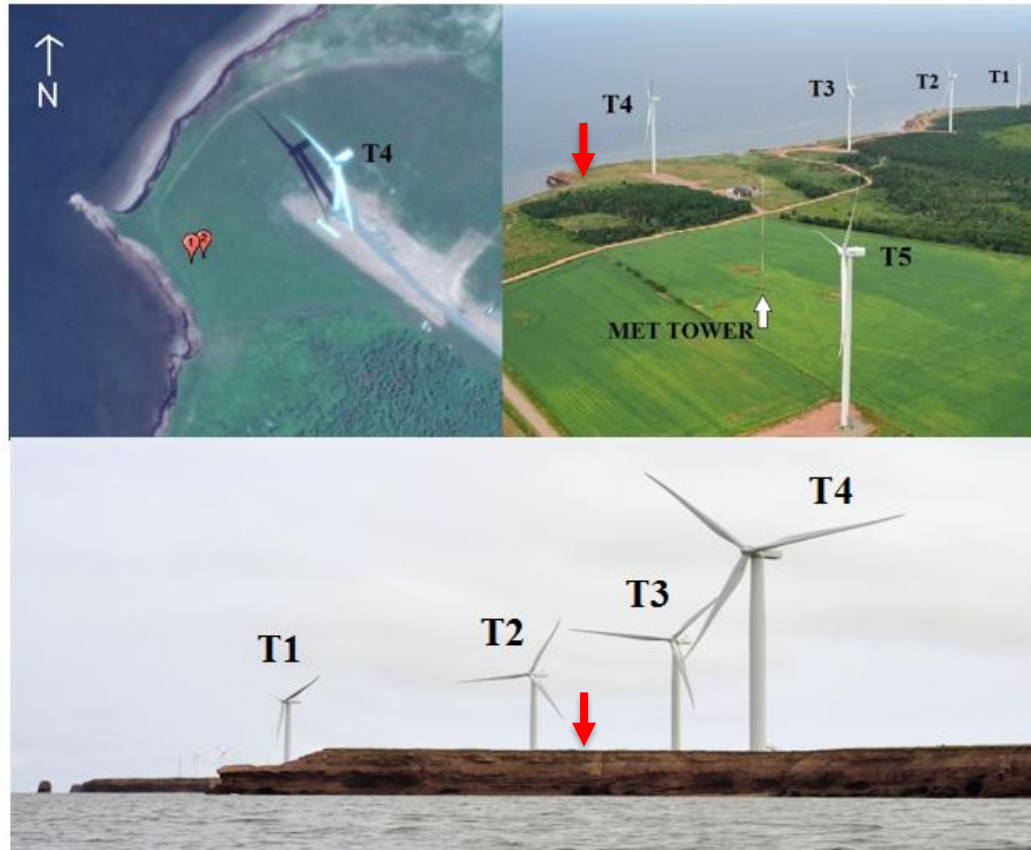
Figure 2-5: Research and Development park, PEI (top right) with windscanner locations (top left) and the escarpment from an upstream point of view (bottom). Red arrows are the location of the windscanner. Photographed by WEIcan.

at the first location and between 2:30 pm to 3:40 pm AST at the second location, while the time between these two measurements was used to reposition the experimental setup. Vertical profiles oriented along the 262° wind direction were scanned at distances of 10, 15, 20, 40 and 80 m from the windscanner up to heights equal to the distance scanned, as depicted in Figure 2-7. The first three profiles were scanned downstream of the escarpment edge while the last two profiles were scanned upstream of the escarpment over the water. At each scan distance, roughly 200 vertical scans were carried out consisting of

measurements at 36 different heights distributed over the scan, for a total duration of 30 seconds. In addition to vertical
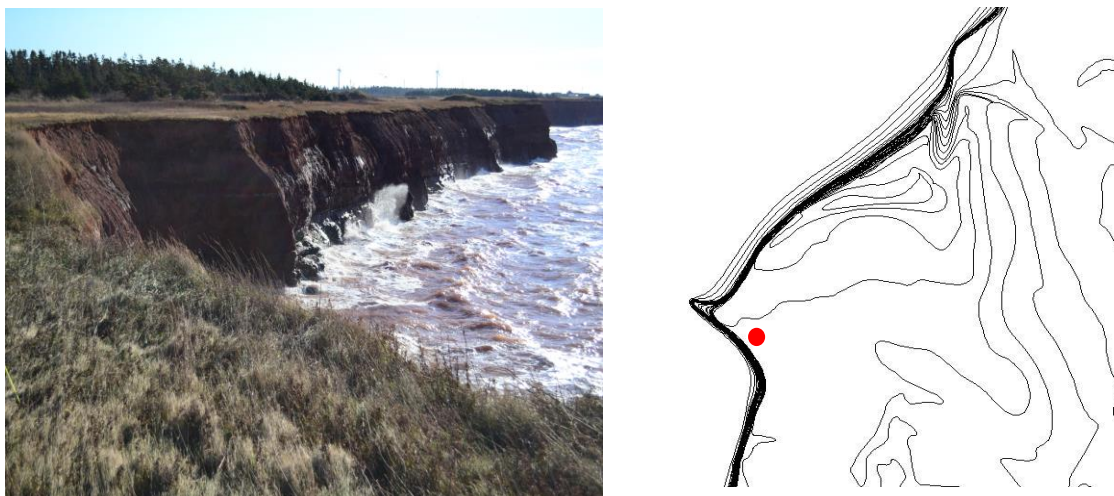
Figure 2-6: Coastal Escarpment at measurement site (left) and contour plot supplied by the Provincial Government of P.E.I. Red marker is the measurement location.

scans, rosette patterns were scanned at each of the distances to provide insight into the local wind direction. Rosette patterns are half spherical shapes scanned ±60˚ from the centerline with a constant focal distance. Each rosette is comprised of roughly 4500 data points. One full scan cycle is comprised of a vertical scan followed by a rosette at each of the locations shown in Figure 2-7. Any scans which had more than eight consecutive measurements of zero were filtered out, which consisted of no more than 15 minutes during each set of measurements. Throughout the afternoon during measurements, the wind direction was predominately from the southwest having a mean direction of 230° (measured from 0° North). Although the windscanner was facing roughly 30° off-axis from the mast measured wind direction, rosette patterns revealed that the inflow to the escarpment was parallel to the 262° axis on which the windscanner was aligned. It is hypothesized that the discrepancy in the wind direction between the two locations may be due to the geometry of the escarpment near the measurement location. The southeastern part of the coastal escarpment, which can partially be seen in Figure 2-5, is roughly 20 m tall and is 370 m west of the MET tower. Aligned with the 225˚ axis, this escarpment is approximately 2.5 km long, southwest the tower's location gradually decreasing in height to 12m with

increasing distance from the research park. Channeling effects may lead the flow to be parallel with this coastline and the MET tower may be close enough to be affected by this behavior.
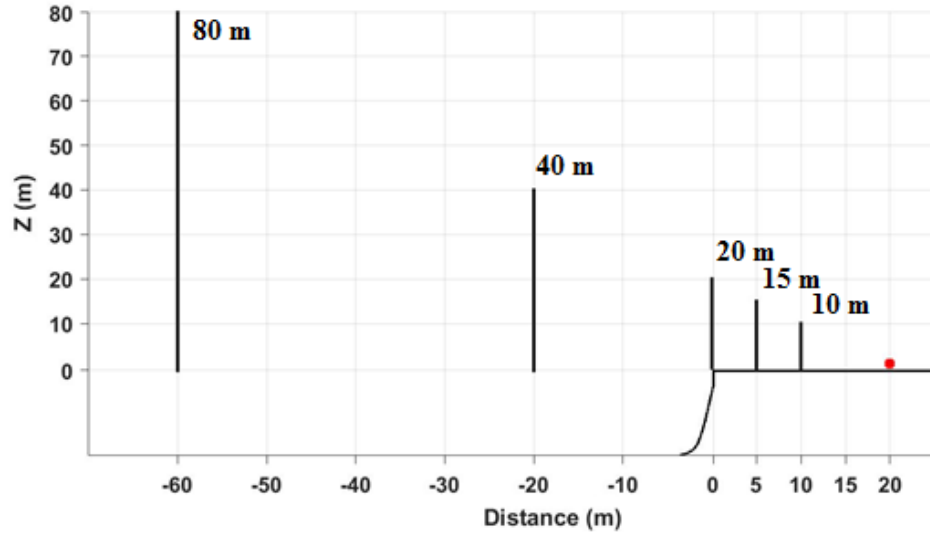
Figure 2-7: Representation of the vertical scans over the escarpment edge at the first measurement location. Distances above vertical scans are horizontal distances from the windscanner, represented by the red marker.

2.3.2 Atmospheric Conditions

The atmospheric stability during the measurement period were calculated using the gradient Richardson number, defined as [20],

$$Ri = \frac{g}{T_o} \frac{\Delta\theta\Delta z}{(\Delta u)^2} \tag{2.2}$$

where, g is gravitational acceleration, T_0 is the surface temperature, $\Delta\theta$ is the potential temperature difference between two points z_2 and z_1 or Δz, and, Δu is the wind speed difference between the same two points. Potential temperature in the previous equation is defined as [37],

$$\theta = T \left(\frac{P_o}{P}\right)^{R/C_p} \tag{2.3}$$

where T is absolute temperature in Kelvin, P_o is standard reference pressure of 1000 mb, P is the atmospheric pressure, R is the gas constant of air and C_p is the specific heat capacity. Using measurements at the tower location between 50 m and the surface at the gradient Richardson number id calculated and is presented in Figure 2-8. It is assumed that the conditions at the tower location and measurement site are similar as they are separated by roughly 500 m. Using stability classifications loosely based on previous studies on the interaction between stability and wind turbines [38], the stability classes are divided into three different categories. In the early afternoon, conditions were neutral ($|Ri| < 0.1$) from 12:30 until 13:00 before transitioning to a very stable state ($0.25 < Ri \leq 1$) from 13:10 – 15:10. In the latter portion of the afternoon, a rapid transition to unstable conditions ($Ri < -0.1$) occurred in the last half hour of measurements. Each measurement period is divided into two sub-sections based on the above stability conditions.
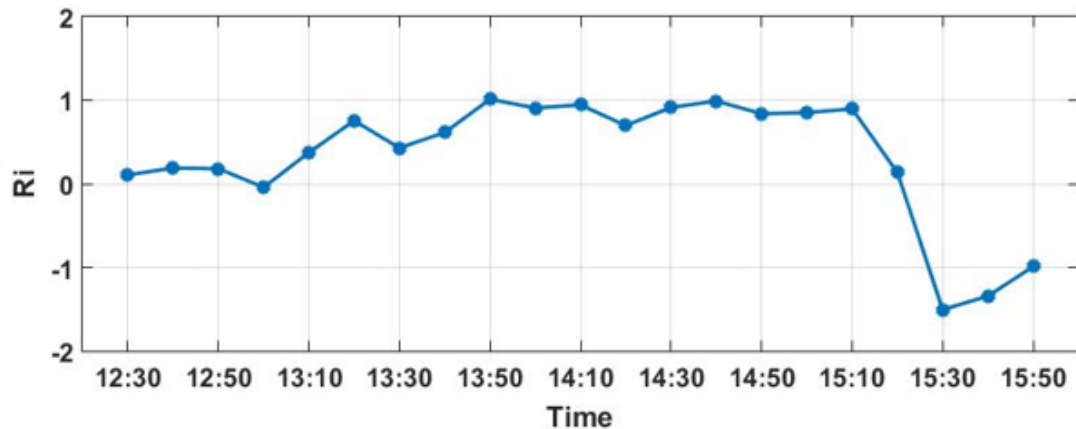
Figure 2-8: Bulk Richardson number during the measurement period on May 15th, 2015

2.4 Results

2.4.1 Mean Velocity

Velocity profiles time-averaged over each stability conduction at all measurement locations are shown in figure 2-8. The escarpment edge is taken to be X = 0 with upstream and downstream distances being negative and positive, respectively. Observed throughout the afternoon were two distinct types of inflow profiles: a sea breeze fronted by a low-level

velocity maxima [39] during the first hour of measurements followed by a transition to a typical boundary layer follow later in the afternoon. Figure 2-8a shows the behavior under neutral sea breeze conditions, where the inflow profile at X = -60 m has a maximum wind speed of 5.2 m/s at a height of approximately 18 m above the surface. In comparison, at a height of 78 m above the surface, where the standard neutral atmosphere log-law wind profile would predict a maximum, the wind speed has a mean of 4.5 m/s. At X = -20 m, the velocity profile shows a similar trend however the wind speeds are moderately reduced beneath the point of maximum velocity at Z = 20 m due to the presence of the escarpment. As the flow strikes the edge of the escarpment a small shear layer forms roughly 3 m above the surface, while the outer flow preserves the characteristics of the sharp maximum in the outer flow. Small magnitudes of reverse flow dropping below -0.2 m/s suggesting a very weak region of recirculation. Moving downstream, the new equilibrium layer begins to merge with the outer flow above the shear layer before likely becoming fully developed

(a)

(b)
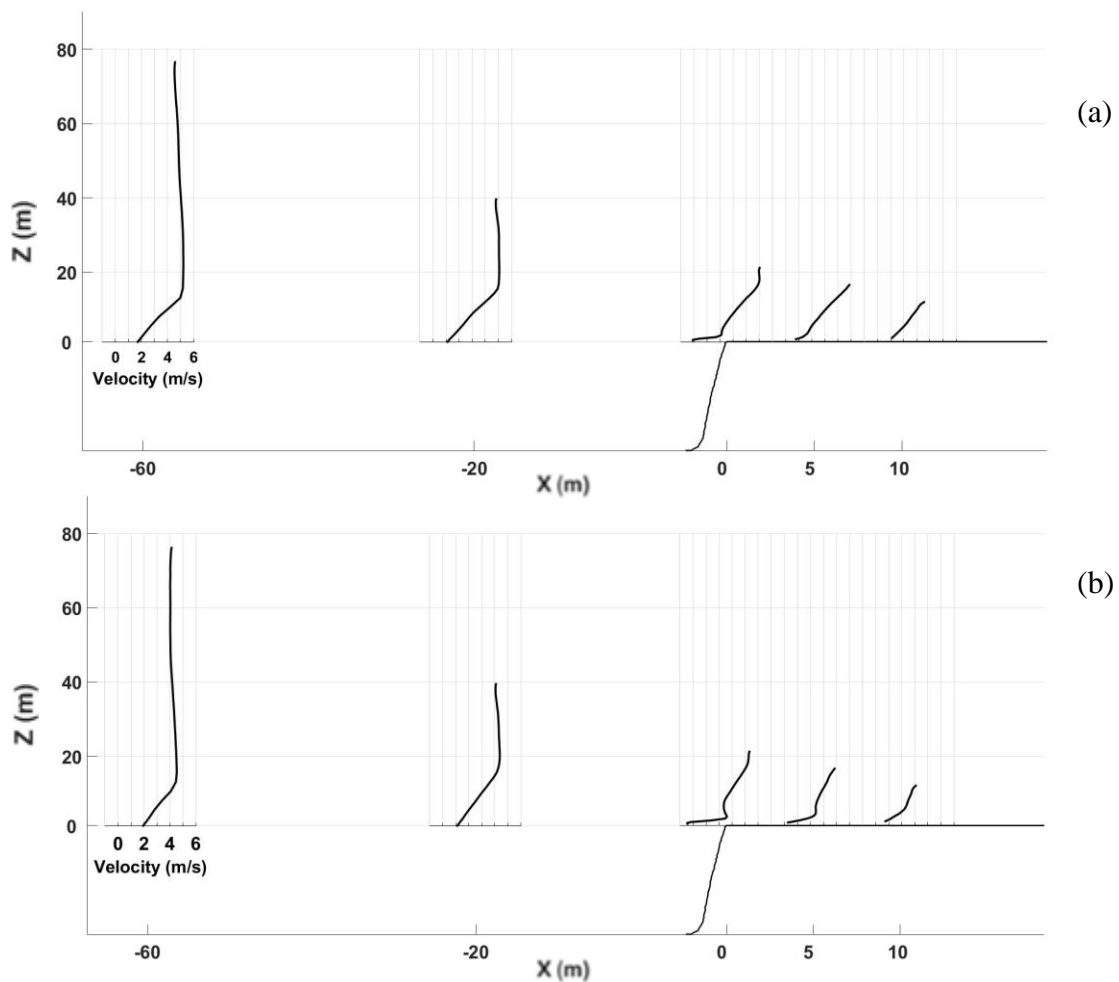
Figure 2-9: Velocity profiles under neutral (a) and stable (b) sea breeze conditions and stable (c) and unstable (d) boundary layer conditions.

at $X = 10$ m. In the same observational period, Figure 2-8b shows the effects of the increasing stability on the sea breeze. It appears that the inhibition of vertical motions has made the sharp low-level maximum more pronounced and increased the degree of the negative shear. A second location of inflection in the wind shear has also appeared at a height of roughly 50 m. With increasing stability, the shear layer formed at the edge of the escarpment becomes more pronounced and produces increased magnitudes of reverse flow suggesting a larger separated region. This leads to near zero velocities at $X = 5$ m from the edge suggesting that the serration and recirculation region extends father downstream. At

X = 10 m from the edge of the escarpment, the surface boundary layer begins to form after reattachment as indicated by the increased gradients near the surface.

In Figure 2-8c, under slightly more stable conditions later in the afternoon as the inflow transitioned to a boundary layer, the velocity profile upstream at X = -55 m hardly shows characteristics of a sea breeze, although there are still large velocity gradients up to a height of 6 m, however, positive shear above this height signals the transition to a typical ABL flow. Downstream of the escarpment edge at X = 5 m, the large low-level gradients produce a shear layer similar to that of the stable sea breeze, however with a less pronounced velocity maximum. A small speed up just above the interface can be identified downstream at X = 10 m.

By the late afternoon, (Figure 2-8d) unstable conditions have caused enhanced vertical motions and have eliminated any signs of the sea breeze from the inflow profile. The development of the flow over the escarpment depicts a growing region of velocity deficit in the lowest parts of the forming boundary layer, with much larger magnitudes of reverse flow compared to any other conditions extending downstream to a distance of 5 m < X < 10 m. This case represents similar behavior to the measurement over the Bolund escarpment using a very similar lidar under neutral stability conditions [22].

2.4.2 Turbulence Intensity

Turbulence intensity profiles over the escarpment for different atmospheric stability conditions are presented in Figure 2-10. Turbulence intensity is defined as the root-mean-square of the instantaneous wind speed normalized by the free stream velocity at the top of each profile [22]. Figure 2-10a shows the turbulence intensity profiles at axial locations of X = 0 m, X = 5 m and X = 10 m from the escarpment in near neutral conditions. Near the surface, the flow is significantly influenced by the geometry of the escarpment, having the greatest turbulence intensity at the escarpment edge reaching up to a peak value of 16%. The overall turbulence intensity profiles remain similar up to a downstream location of X=5 m, beyond that there was an overall increase in turbulence intensity. At X = 10 m, the turbulence intensity magnitude was about 6% higher than that at X = 5m possibly due to
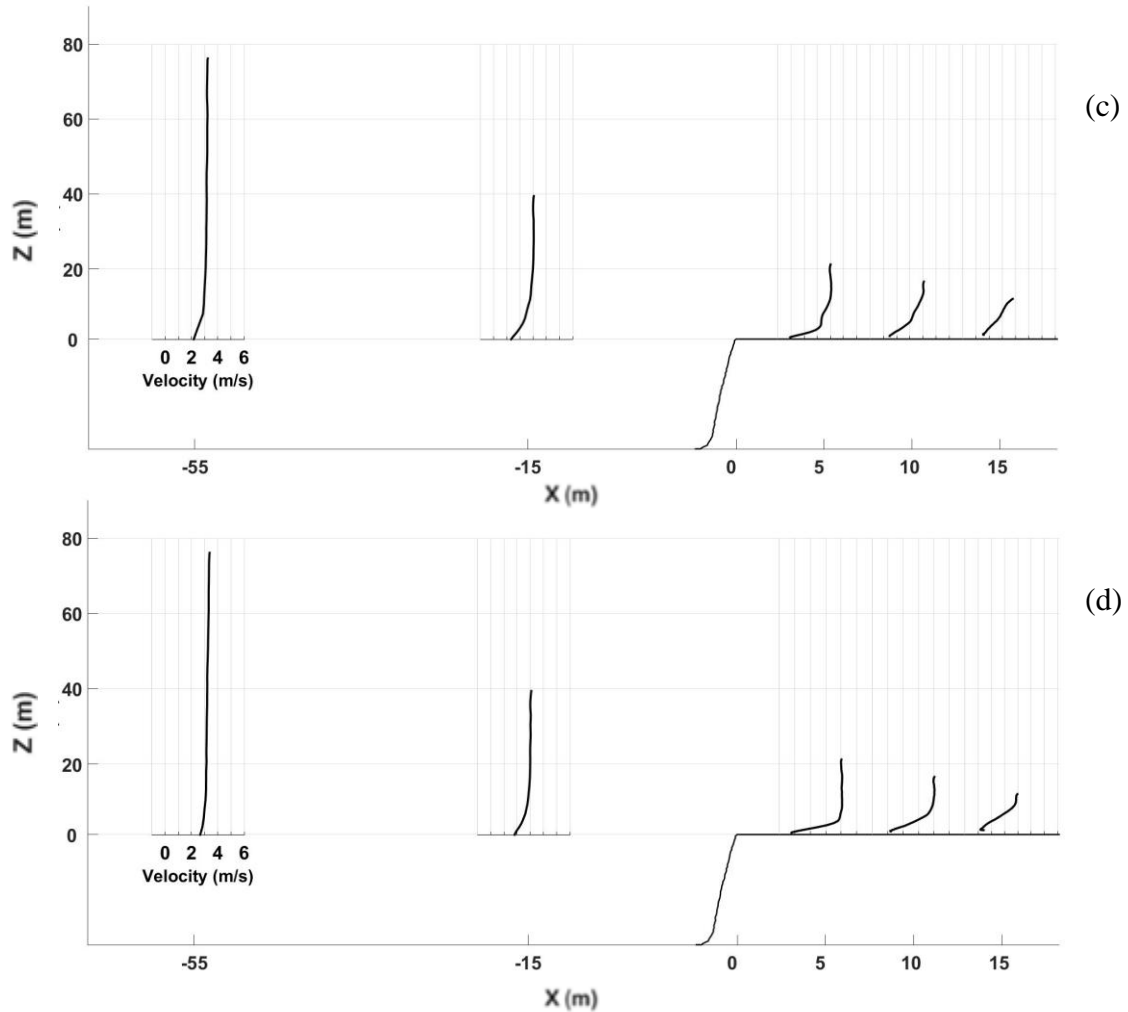
Figure 2-10: Turbulence Intensity profiles under neutral (a) and stable (b) sea breeze conditions and stable (c) and unstable (d) boundary layer conditions.

the formation of the new boundary layer. Interestingly, a small increase in turbulence intensity at the edge of the escarpment is seen at a height of 15 m, which coincides with the peak of maximum velocity of the sea breeze profile seen in Figure 2-10a. The sea breeze front has essentially created a second layer of increased turbulence which begins to show itself in the increasing turbulence 10 meters onshore, which may be indicative of the convective internal boundary layer forming.

As the sea breeze conditions became more stable and as the wind speed continued to decrease, the effects of the escarpment geometry on the turbulent flow are amplified as shown in Figure 2-10b. The results show the presence of two regions with distinct turbulent behavior. The bottom region adjacent to the surface has enhanced turbulent magnitudes. This region started to extend in both height and magnitude with an increase in the

downstream distance. The location of the peak turbulent intensity also started to move away from the surface. In the other region above this, the turbulent intensity gradually started to increase with height. The results show that, similar to the bottom region, the turbulent intensity in this region also started to increase with the downstream distance, however, the location of turbulent intensity peak tends to move towards the surface. On average, the turbulent intensity magnitude increased by 8% from X=0 to X=10m for the stable case.

Later in the afternoon, upstream measurements made from the second location of the windscanner show a stable period in which the upstream velocity profile started to change from sea breeze to the typical ABL. This has caused a change in the turbulent flow behavior over the escarpment as evident in Figure 2-10c. The results indicate that the two turbulent regions observed earlier, were merged to form an enhanced turbulent near-surface region that extended to a height of approximately 10 m above the ground. The overall turbulence magnitudes in this region were higher than that observed previously. Outside this region, turbulent intensity drops sharply by more than 50%. The results also indicate an overall increase in the turbulent intensity with an increase in the downstream distance but the percentage increase is lower than that observed for the stable condition with a sea breeze inflow.

In the unstable regime, in Figure 2-10d which favors vertical motions, the absence of gusts as well as the sea breeze, the turbulent flow over the escarpment became similar to that expected over a sharp-edged bluff body. That is, the turbulence enhancement was restricted to the near-surface region that experienced the flow separation by the escarpment edge. The turbulent intensity in this region was highest among all stability conditions, with the peak magnitude reaching about 35%. While in the free stream region above this layer, the turbulent intensity drops to about 5%.

2.4.3 Effect of Inflow on Wake Height

Dependence of the wake flow on wind speed is difficult to determine, as the consistently decline wind speed throughout the measurement were coupled with stability changes, as well as the change from a sea breeze flow to a boundary layer flow. Therefore, the behavior

in the wake of the escarpment under the presented inflow conditions will be investigated through examining the boundary between the inner and outer layers of the flow downstream of the escarpment during the measurements under stability classes defined in section 3.2. Figure 2-11 displays a time series of velocity profiles over one scan cycle (30 seconds) at a distance of X = 10 m from the edge of the escarpment, to directly compare the near surface behavior below Z = 10m. This position was chosen as it is one of the two overlap regions (X = 5 m and X = 10 m) between the two sets of measurements and as each scanned location consisted of roughly 36 points over the scanned height, the shortest scan considered here has the highest spatial resolution. As part of the programming of this scanning pattern, there were no measurements take near the surface, which is the reason for the missing data. As these are essentially snapshots of the velocity profiles in time, it is difficult to directly compare the characteristics as an absolute, but the trends of the stability conditions are clearly definable. In general, under sea breeze inflow conditions there is a significantly less, if any, of reverse flow compared to the boundary layer inflow while having velocity deficits extending to greater heights from the surface. Among the sea breeze cases, the frequency of reverse flow regions of neutral measurements is less than that for stable conditions which is depicted in Figures 2-11a and 2-11b. Under boundary layer conditions, the effect of the atmospheric stability is again depicted here, with unstable conditions creating a marginally larger reverse flow region which appears to be more consistent throughout the measurements.

These high-resolution measurements allow for the determination of the wake height based on the four stability and inflow conditions discussed earlier. The wake height, h, can be defined using two different methods. Method 1 calculates the displacement thickness, which is the height that the boundary layer is displaced to make up for the reduction in mass flow rate caused by the boundary layer and is given as:

$$h_1 = \int_0^{Z_{max}} (1 - \frac{u(z)}{U_o}) \tag{2.4}$$

where $u(z)$ is the wind speed at height z, and U_o is the free stream velocity [40]. Method 2 identifies the wake height as the maximum wind speed gradient [41] and is given as:

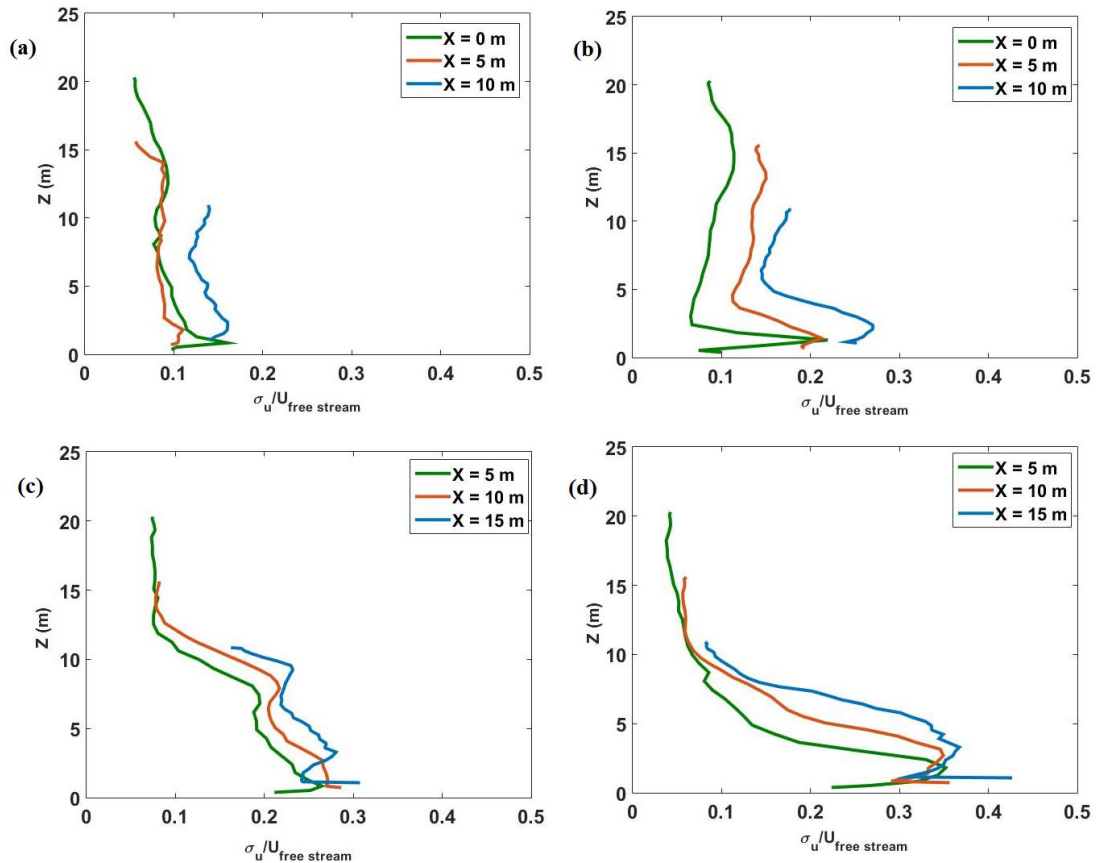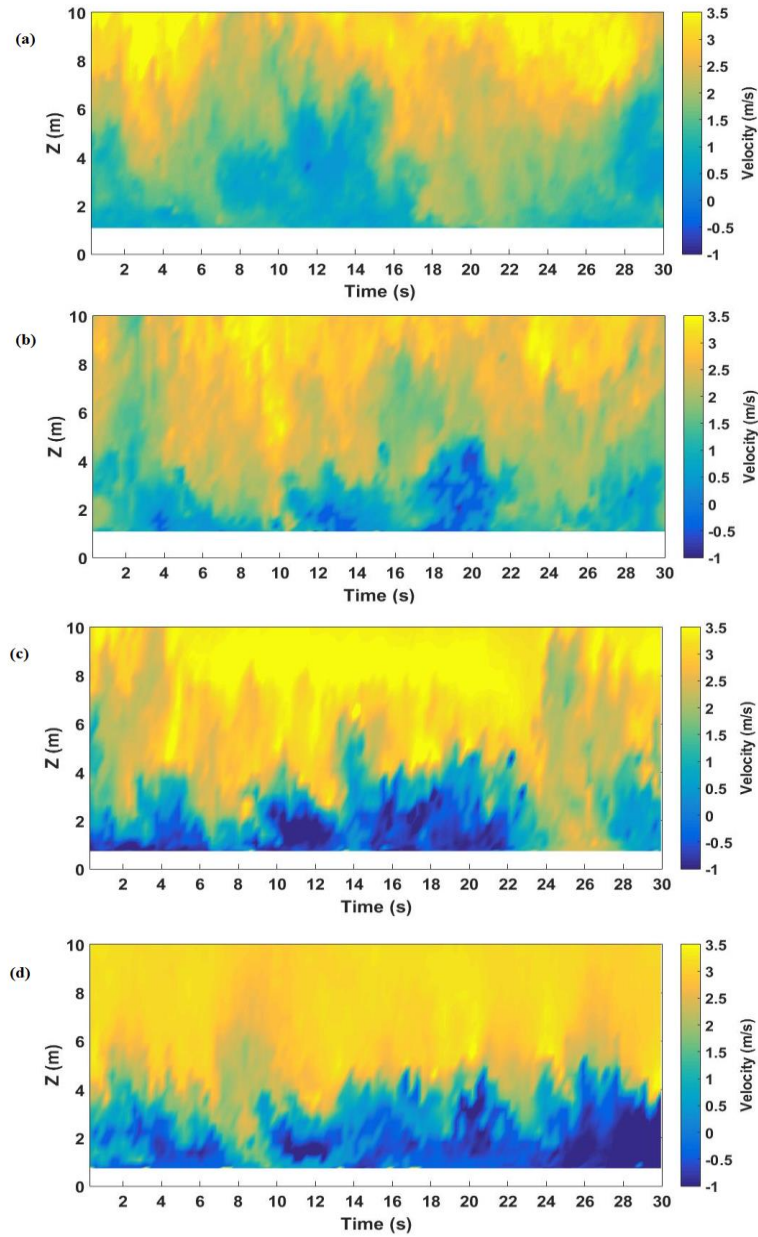**Figure 2-11: Instantaneous velocity profiles over one scan cycle at X = 10 m from the escarpment edge under neutral (a) and stable (b) sea breeze conditions and stable (c) and unstable (d) boundary layer conditions.**

$$h_2 = \arg\max_z(\frac{du(z)}{dz})$$ (2.5)

The mean wake height calculated using the two methods are presented in Figure 2-12 for each of the four-different stability and inflow conditions. Both methods show very similar

trends with method 2 often providing larger values for each condition. The standard deviation is larger using method two as the point of maximum gradient can be quite variable, particularly in the case of the sea breeze inflow. Figure 2-12 shows, under see breeze inflow behavior for both neutral and stable conditions, the wake size variations are similar. That is, the wake height is largest at the edge of the escarpment, which decreases moving downstream. On the other hand, when the inflow transitioned to a boundary layer under stable and unstable conditions, wake size variations reversed. That is, the wake height is lower at the leading edge, which increased with the downstream distance, which is typical in a flow over an escarpment under ABL inflow [26]. Figure 2-12 implies that the wake height has strong dependency on the inflow profile and weak dependency on atmospheric stability.
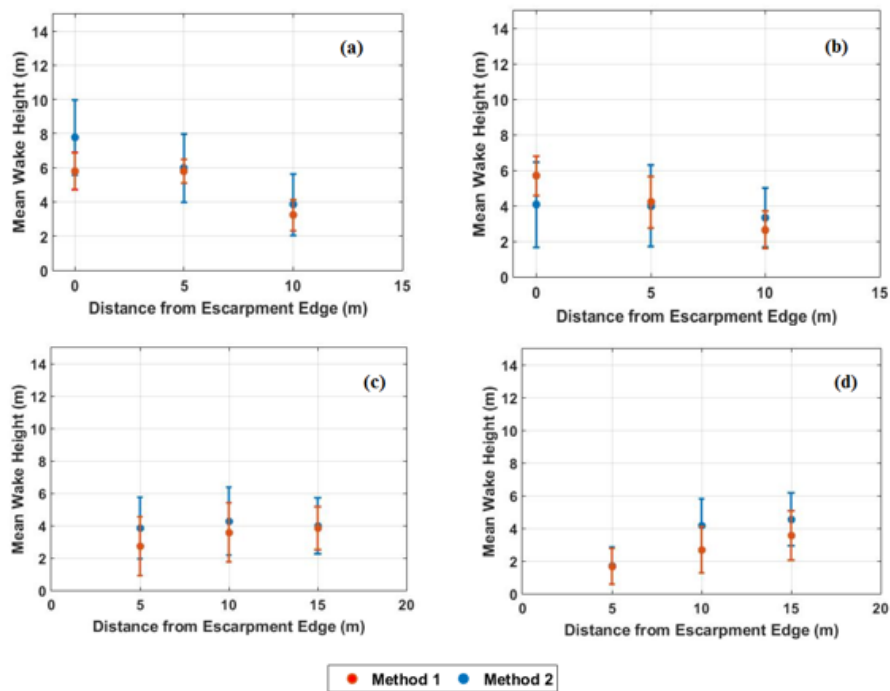
Figure 2-12: Mean wake height estimated using both methods for neutral (a) and stable (b) sea breeze conditions and stable (c) and unstable (d) boundary layer conditions. The error bars displayed represent the standard deviation of each method.

2.4.4 Inflow Effects on Turbine Power

The upstream vertical profiles over the water, i.e. 80 m upstream of the windscanner provide hub height (78 m) wind speed measurements which are difficult to measure in traditional mast setups. The International Electrotechnical Committee (IEC) provides guidelines for power performance analyses and states that measurements should be taken 2-4 rotor diameters upstream of the turbine [42]. Although the farthest upstream measurements taken are roughly 10 m under this distance, it is still useful to compare the unique sea breeze inflow to some relevant turbine parameters such as wind speeds at hub height, active power and power fluctuations. During the measurement period on May 15th, the nacelle of the turbine was directing along the 245° axis and 220° axis during the first and second measurement period respectively, which is roughly 20° and 45° off axis of the line of sight of the windscanner. As inflow to turbine 4 at the measurement site was perpendicular to the escarpment, the measurements from the cup anemometer on the hub should be less affected by the turbine blades while the nacelle is turned. The cup anemometer on the turbine nacelle sampled at 1 Hz and the data is logged as 10-minute averages. The sampling rate of the wind scanner is 250 Hz, as previously mentioned, but at one point within the scan the effective sampling frequency, taken as the number of samples at a point over the scan period, is roughly 6.67 Hz for the heights presented. Additionally, the upstream measurements from the windscanner are cyclic and hence separated by roughly 4.5 minutes before returning to the same position. Figure 2-13 presents the hub height speeds measured upstream and at the turbine location as well as the wind speed at half-hub height (40 m) which is within the lower tip radius of 33.5 m from the surface. Additionally, the recorded turbine power output and fluctuations in turbine power output during the same period are presented. Observations upstream show a relatively good agreement in the neutral sea breeze (12:30– 13:00), and boundary layer inflow conditions, while deviating from cup anemometer measurements under the stable wind speeds measured upstream and at the turbine location as well as the wind speed at half-hub sea breeze inflow conditions (13:00 – 13:30). The results show that during the sea-breeze conditions the wind speed at 40 m is greater than that of hub height. The length of time in which the neutral sea breeze inflow conditions occurred, a significant spike in power fluctuations is seen between 12:40 – 12:50 while the power is decreasing. The

standard deviation of power output increased from 19 kW to 34 kW while the wind speeds at hub height decrease slightly during this time. The increase in the fluctuations by approximately 80% during this 10-minute interval, is closely related to the gust observed in the sea breeze profile under neutral conditions presented in Figure 2-14a. During this 10- minute period, the mean wind speed at 80 m was 4.37 m/s while the wind speed at 40 m was 5.27 m/s giving a cubed ratio equal to 0.74. As this ratio is very close to the observed increase in the power fluctuations, it is reasonable to assume that the larger fluctuations are caused by the gust. It is also likely that this low-level maximum influenced the active power, but due to the wind speeds dropping below the cutoff wind speed (4.5 m/s) the turbine was braking to a halt.
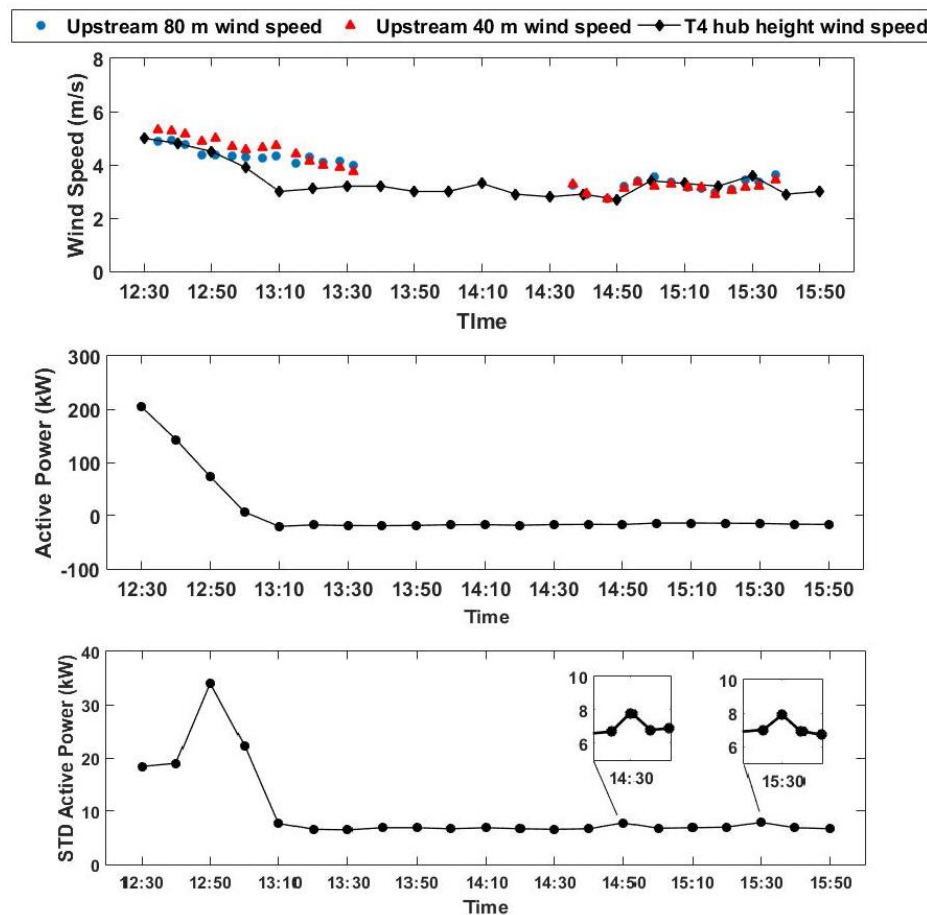
Figure 2-13: Windscanner measurements at hub height (80 m) and half hub height (40 m) upstream of the escarpment compared to the turbine anemometer(a) turbine active power (b) and standard deviations of active power (c).
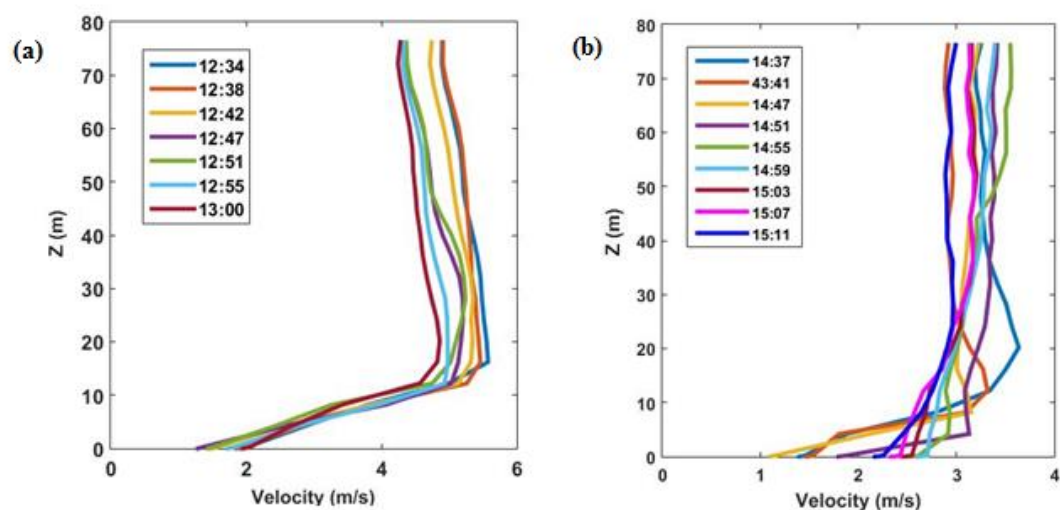
Figure 2-14: Velocity profiles of individual scanned cycles (30 seconds) during the measurement period with neutral stability (a) and stable (b) conditions.

caused by the gust. It is also likely that this low-level maximum influenced the active power, but due to the wind speeds dropping below the cutoff wind speed (4.5 m/s) the turbine was braking to a halt.

2.5 Conclusions

A field campaign was conducted at the Wind Energy Institute of Canada's Research and Development park where five 2MW wind turbines are sited near a 14 m coastal escarpment. The aim of the campaign was to investigate the influence of the coastal escarpment and wind turbine wakes at different scales. Herein, a windscanner scanning Lidar developed by DTU was used to measure vertical wind shear profiles extending up to hub height and half-hub height upstream of the escarpment. Additionally, flow over the escarpment was measured below 20 m to characterize the near surface flow field. This field study provides insight into the influence of inflow profile as well as the atmospheric stability condition on the flow over the escarpment that may influence the turbine performance.

The upstream inflow conditions have a significant impact on the mean flow field in the near surface region downstream of the escarpment edge. When compared to typical boundary layer flow, as seen in unstable conditions in the late afternoon, the sea breezes formed an initially stronger, larger shear layer at the escarpment edge which decayed relatively quickly. A clear division between the inner wake region and outer layer is evident in these flows. The wake formed downstream of the escarpment under sea breeze conditions decayed downstream, contrary to that seen in the boundary layer flow. Moreover, a second layer, aside from the geometry dominated near surface region, is present with a sea breeze inflow indicating that this front is highly turbulent. This secondary turbulent region penetrates inland with the tendency to increase in intensity and decrease in height, possibly combining with the near surface wake, when there are large velocity gradients in the lowest portion of the inflow profile. On the other hand, in stable stratification when the sea breeze is transitioning into a boundary layer and the gradients became weaker, the near-surface turbulent layer extended.

Turbine 4 nearest to the measurement location saw a significant spike in power fluctuations of roughly 80% during the measurement period. Upstream inflow profiles captured a gusty period of roughly 10 minutes embedded within the neutral sea-breeze profile which had its peak velocity at roughly 40 m, within the lower radius of the rotor diameter. As the sea breeze penetrated inland, the lower rotor radius was subjected to this increased wind speed, which is likely the cause for this increase in the power fluctuations.

This study identifies that non-ABL inflow conditions, such as sea breezes, can significantly influence the near surface mean and turbulent flow characteristics. Point measurement systems are often difficult to place in areas off the coast, which introduced uncertainty in predicting inflow conditions over coastal topography and wind farms. Although a simple measure of stability from a met mast may characterize the thermal effects on the site, modification of the log-law to take into account stability effects not necessarily provide accurate inflow characterization. Furthermore, this highlights the variability of full-scale measurements and the advantages of remote sensing in coastal areas.

References

[1] Gasset, N., Landry, M., and Gagnon, Y., 2012. A comparison of wind flow models for wind resource assessment in wind energy applications. Energies, 5, 4288–4322.

[2] Palma, J. M. L. M., Castro, F.A., Ribeiro, L.F., Rodrigues, A.H., and Pinto, A.P., 2008. Linear and nonlinear models in wind resource assessment and wind turbine micro-siting in complex terrain. Journal of Wind Engineering and Industrial Aerodynamics, 96, 2308–2326

[3] Bechmann A., Sørensen, N.N., Berg J., Mann J., and Réthoré, P.-E., 2011. The Bolund experiment, part II: blind comparison of microscale flow models. Boundary-Layer Meteorology, 141, 245–271.

[4] Rowcroft, J., Burton, D., Blackburn, H.M., Sheridan, J., 2016. Siting wind turbines near cliffs − the effect of wind direction. Wind Energy, 19: 1469-1484.

[5] Emeis, S., Frank, H., Fiedler, F., 1995. Modification of air flow over an escarpment. Results from the Hjardemål experiment. Boundary-Layer Meteorol 74(1–2):131–161

[6] Chaudhari, A., Hellsten, A., Hämäläinen, J., 2016. Full-Scale Experimental Validation of Large-Eddy Simulation of Wind Flows over Complex Terrain: The Bolund Hill. Advances in Meteorology. 2016: 1-14

[7] Walmsley, John L., and Peter A. Taylor., 1996. Boundary-Layer Flow over Topography: Impacts of the Askervein Study. Boundary-Layer Meteorology, vol. 78, no. 3-4, pp. 291–320.

[8] Mickle, R. E., Cook, N. J., Hoff, A. M., Jensen, N. O., Salmon, J. R., Taylor, P. A., Tetzlaff, G., and Teunissen, H. W., 1988. The Askervein Hill Project: Vertical Profiles of Wind and Turbulence. Boundary-Layer Meteorology 43.1-2: 143-69.

[9] Silva Lopes, A., Palma, J.M.L.M., Castro F.A., 2007. Simulation of the Askervein flow. Part 2: large-eddy simulations. Boundary-Layer Meteorol 125(1):85–108.

[10] Chow, F.K., Street, R.L., 2009. Evaluation of turbulence closure models for large-eddy simulation over complex terrain: flow over Askervein Hill. J Appl Meteorol Climatol 48(5):1050–1065.

[11] Teunissen, H.W., Shokr, M.E., Bowen, A.J., Wood, C.J., Green, D.W.R., 1987. The Askervein Hill Project: wind-tunnel simulations at three length scales. Boundary-Layer Meteorol 40(1–2):1–29.

[12] Bradley, E.F., 1980. An experimental study of the profiles of wind speed, shearing stress and turbulence at the crest of a large hill. Quart. J. Roy. Meteorol. Soc. 106, 101–124.

[13] Salmon, J.R., Teunissen, H.W., Mickle, R.E., Taylor, P.A., 1988. The kettles hill project: Field observations, wind-tunnel simulations and numerical model predictions for flow over a low hill. Boundary Layer Meteorology 43, 309–343.

[14] Mason, P.J., 1986. Flow over the summit of an isolated hill. Boundary Layer Meteorology 37, 385–405.

[15] Jensen, N., Peterson, E., 1978. On the escarpment wind profile. Q J R Meteorol Soc 104(441):719–728.

[16] Jackson, P. S., and Hunt, J. C. R, 1975. Turbulent Wind Flow over a Low Hill. Quarterly Journal of the Royal Meteorological Society 101.430: 929-55.

[17] Bowen, A., 1979. Some effects of escarpments on the atmospheric boundary layer. PhD Dissertation, University of Canterbury

[18] Bowen, A. J., and Lindley, D., 1977. A Wind-Tunnel Investigation of the Wind Speed and Turbulence Characteristics Close to the Ground over Various Escarpment Shapes, Boundary-Layer Meteorol. 12, 259-271.

[19] Adrian, G., and Fiedler, E., 1991. Simulation of Unstationary Wind and Temperature Fields over Complex Terrain and Comparison with Observations, Beitr. Phys. Atmosph. 64, 2748.

[20] Berg, J., Mann, J., Bechmann, A., Courtney, M., Jørgensen, H., 2011. The Bolund experiment, part I: flow over a steep, three-dimensional hill. Boundary-Layer Meteorol 141(2):219–243

[21] Mann, J., Angelou, N., Sjöholm, M., Mikkelsen, T., Hansen, K. H., Cavar, D., Berg, J., 2014. Laser Scanning of a Recirculation Zone on the Bolund Escarpment. Journal of Physics: Conference Series 555: 012066.

[22] Lange, J., Mann, J., Angelou, N., Berg, J., Sjöholm, M., Mikkelsen, T., 2015. Variations of the Wake Height over the Bolund Escarpment Measured by a Scanning Lidar. Boundary-Layer Meteorology 159.1: 147-59.

[23] Barthelmie, R.J., Palutikof, J.P., 1996. Coastal Wind Speed Modelling for Wind Energy Applications. Journal of Wind Engineering and Industrial Aerodynamics 62, 213-236.

[24] Miller, S. T. K., 2003. Sea Breeze: Structure, Forecasting, and Impacts. Reviews of Geophysics 41.

[25] Berge, E., Gravdahl, A.R., Schelling, J., Tallhaug, L., Undheim, O., 2006. Wind in complex terrain. A comparison of WAsP and two CFD-models. Proceedings from EWEC, Athens Greece.

[26] WAsP 10 Help Facility and On-line Documentation. s.l. : Risø National Laboratory, 2007.

[27] Angelou, N., Mann, J., Sjöholm, M., Courtney, M., 2012. Direct measurement of the spectral transfer function of a laser based anemometer. Rev Sci Inst 83(3):33,111

[28] Karlsson, C., Olsson, F.A., Letalick, D., Harris, M., 2000. All-fiber multifunction continuous-wave coherent laser radar at 1.55 μm for range, speed, vibration, and wind measurements. Appl Opt 39(21):3716–3726.

[29] Mikkelsen, T., Mann, J., Nielsen, M., 2011. Rotating prism scanning device and method for scanning. Patent No.: WO 2009/155924 A1, 2009.

[30] Sjöholm M., Angelou N., Hansen P., Hansen K.H., Mikkelsen T., Haga S., Silgjerd J., Starsmore N., 2014 Two dimensional rotorcraft downwash flow field measurements by lidar-based wind scanners with agile beam steering. J Atmos Ocean 314:930–937

[31] Sonnenschein, C., Horrigan, F.A., 1971. Signal-to-noise relationships for coaxial systems that heterodyne backscatter from the atmosphere. Appl Opt 10(7):1600

[32] Angelou N, Mann J, Sjöholm M, Courtney M (2012) Direct measurement of the spectral transfer function of a laser based anemometer. Rev Sci Inst 83(3):33,111

[33] Abari CF, Pedersen AT, Dellwik E, Mann J (2015) Performance evaluation of an all-fiber image-reject homodyne coherent Doppler wind lidar. Atmos Meas Tech 8(4):3729–3752. doi:10.5194/amtd-8-3729-2015

[34] Hangan, H., 2014. The Wind Engineering Energy and Environment (WindEEE) Dome at Western University, Canada. Wind Engineers, JAWE, 39:4(141).

[35] van Dooren, M. F., Kahn, M., Petrovic, V., Bottasso, C. L., Campagnolo, F., Sjöholm, M., Angelou, N., Mikkelsen, T., Croce, A., Zasso, A., 2016 Demonstration of Synchronised Scanning Lidar Measurements of 2D Velocity Fields in a Boundary-layer Wind Tunnel." Journal of Physics: Conference Series, 753, 72032. doi:10.1088/1742-6596/753/7/072032.

[36] Barthelmie, R.J., Wang, H., Doubrawa, P., Giroux, G., Pryor, S.C., 2016. Effects of an escarpment on flow parameters of relevance to wind turbines. Wind Energy 2016. 19:2271-2286

[37] Kaimal, J. C., and J. J. Finnigan. 1994. Atmospheric Boundary Layer Flows: Their Structure and Measurement. New York: Oxford UP.

[38] Kelley, N. D., 2011, Turbulence-Turbine Interaction: The Basis for the Development of the Turbsim Stochastic Simulator, Technical Report No. TP-5000- 52353, National Renewable Energy Laboratory, Golden, CO.

[39] Helmis, C. G., Asimakopoulos, D. N., Deligiorgi, D. G., & Lalas, D. P. (1987). Observations of sea-breeze fronts near the shoreline. Boundary-Layer Meteorology,38(4), 395-410. doi:10.1007/bf00120854

[40] Pope, S.B., 2000. Turbulent flows. Cambridge University Press, Cambridge.

[41] Emeis S, Schäfer K, Münkel C (2008) Surface-based remote sensing of the mixing-layer height—a review. Meteorol Z 17(5):621–630. doi:10.1127/0941-2948/2008/0312

[42] International Electrotechnical Commission. International standard, IEC61400 Wind turbine generator systems – Part 12: wind turbine power performance testing. IEC 61400-12:1998(E). In IEC 61400-12 First edition 1998-021998. IEC, FDIS: Geneva, Switzerland, 2005; 60.

Chapter 3

3   Experimental Investigation of Impact of Inflow conditions and Local Topographic Features on a Coastal Escarpment

3.1   Introduction

With the growth of the wind energy sector, wind turbine installations in complex terrains outside the typical flat and homogenous territories, are becoming more common. Complex terrain comprises large-scale features such as hills, escarpment and forest canopies that are characterized by significant abrupt changes in local elevation [1]. These features are often associated with local wind speed-ups, and hence may be advantageous from a wind potential aspect [2]. However, these increased wind resources are at the expense of three-dimensional modifications to the flow which include regions of high vertical velocities, flow separation, shedding vortices and enhancement of turbulence [3, 4]. Hence, the local topographic features can have a significant impact on the performance as well as lifespan of a wind turbine.

Coastlines are becoming potential options for wind farm siting due to their long open-water fetches for higher wind speeds [5]. An escarpment or cliff is a common topographic feature along shorelines and hence its impact of the flow approaching a wind turbine needs to be properly accounted for when designing a wind farms and evaluating its performance and financial feasibility. The wind speed is of the utmost importance as the power output of a wind turbine is related to the cube of the wind speed, and more accurately, the weighted-average wind speed over the rotor diameter [6, 7]. Industry standard linearized models, such as WAsP, for wind resource assessment and wind turbine micro-siting have proven to predict the onsite conditions in homogenous terrain with accuracy, but often fail to provide reliable results in areas of complex terrain [1, 8]. Despite the inaccuracies, these linear models are often chosen for their moderate computational cost and user input compared to more intricate, computationally intensive models such as Reynolds Averaged Naiver-Stokes (RANS) or Large Eddy Simulation (LES) [9, 10]. The increase in computing power has begun the transition to more complex modelling techniques, but the correct

parameterization of the models used in simulations for complex terrains, is vital for the accuracy of model predictions. Therefore, to improve computational modeling of flow in complex environments, the characteristics of the flow must be fully understood from a fluid dynamics perspective to allow users to appropriately select boundary conditions and tune turbulence models.

Full-scale measurements of flow in complex topography are often limited by instrumentation and logistical challenges. For example, the most common mast instrumentation i.e. the cup anemometer, often do not serve well in complex terrain due to the inherent measurement errors [11]. New technological advances in the areas of remote sensing have increased the capability to accurately measure flow regimes in complex terrain, however, these instruments are substantially more expensive than cup anemometers. Regardless of the instrumentation used, lack of control of the environmental conditions and repeatability are limiting factors when conducting full-scale measurements. Thus, wind tunnels are often used as a viable mean to reproduce environmental flows at smaller scales in a controlled environment. The experimental data from wind tunnel studies is also a viable resource to validate numerical models [13].

During the last few decades, an increased amount of attention has been turned toward flow over hills and escarpments. Most of the reported wind tunnel studies concentrated on simpler, two dimensional geometries with modest slopes and most three-dimensional studies were conducted on axis symmetric models. These studies often were limited to measure of mean velocity, or speed-up ratio, at the crest of the topographic feature.

Flow over two-dimensional, gentle hills with slopes ranging from 10° - 26° was studied by Arya et al. [14]. The study was focused on gaining a better understanding of the relationship between the hill slope and flow dispersion on the leeside of the hill. The speed-ups observed at the crest were found to be proportional to the slope of the hill. Kim et al. [15] conducted wind tunnel study on four different cosine shaped hills in isolated and series format and the resulting velocity profiles and turbulent kinetic energy were compared to linear and numerical results. It was observed that a smaller neighboring hill in the presence of a taller hill does not affect the mean velocity profile at the hill crest while the opposite is true for

a tall hill neighboring a smaller hill. The numerical models showed good agreement in predicting the mean velocity profiles. Carpenter and Locke [16] performed a wind tunnel study on the flow over a multitude of two dimensional hills in both single and consecutive configuration at 1:1000 scale. The steepest hills used has a slope of roughly 26° and the shallowest was 14°. Results of the mean flow speed compared well with results from a numerical model when the flow separation was limited. The numerical model however, did not show good agreement with the rms turbulent velocity.

The physical modelling of real topographies has also been reported in the literature. Several benchmark full-scale field experiments have been extended into the wind tunnel domain for the purpose of investigating wind resource assessment and/or wind turbine micro-siting. Askervein hill [17] was modelled at three different length scales (1:800, 1:1200, 1:2500) which showed that, regardless of scale, the flow characteristics such as speed up and turbulence intensity due to small scale features agreed with full-scale data. The Kettles hill [18] experiment showed that the wind tunnel model results tended to overpredict the speed-up at the crest and showed a low-level maximum which was not observed in the field, suggesting that the field measurements were not low enough to capture the point of maximum velocity. Similarly, flow over multiple hills and valleys have also been reported in the literature such as Rasouli et al. who conducted Particle Image Velocimetry (PIV) over a topographic model of the surrounding terrain of Hong Kong [19,20]. The most recent field campaign was done over the 12 m Bolund escarpment in Denmark [21]. This experiment arose from the need for more benchmark cases to validate numerical models. Wind tunnel testing has previously been conducted, comparing the results of mean flow and turbulent kinetic energy to the full-scale data [22] and the most recent efforts were conducted by Kilpatrick et al. [23]. The influence of upstream conditions on the flow over the escarpment was investigated using PIV and it was concluded that a better comparison to full-scale in terms of turbulent kinetic energy was obtained using the unique abilities of the Wind Engineering, Energy and Environment (WindEEE) dome. Many physical and numerical simulations that have been conducted on this escarpment showed a wide variety in the results indicating that there is a need to further improve the accuracy of modelling over steep, complex terrain and herein lies the motivation for this study.

The present study is focused on the characterization of the flow field over a 1:50 scale model of a coastal escarpment located on a wind farm located in Prince Edward Island, in a laboratory setup. Two different inflow conditions were considered and the influence of local topographic features of the escarpment on the flow propagation towards a local turbine was studied in detail.

3.2 WindEEE

The experiments were conducted in the WindEEE Dome, which is the world's first three-dimensional wind chamber with the ability to physically simulate both synoptic and non-synoptic wind flows at large scales. The wind chamber is hexagonal in shape (25 m diagonal length) and operates in a closed-return mode inside a larger outer chamber of 40 m diagonal length. The test chamber contains 106 fans, each of which can be controlled individually via variable frequency drives to produce a range of synoptic and non-synoptic flow conditions. Of the 106 fans, 60 fans are oriented in an array of 4×15 on one of the six chamber walls. The remaining 46 fans are divided amongst the remaining five walls (8 fans per wall) and the upper plenum (6 fans). Each fan has a diameter of 0.8 m and can produce a maximum velocity of approximately 25 m/s at a power of 30 kW. Additionally, roughness elements, grouped into zones inside the chamber, can be positioned at specific heights to simulate a large range of atmospheric boundary layer flows. In total, the chamber has over 1500 roughness elements each with a maximum height of 30 cm. A full description of the test facility can be found in Hangan [24].

3.3 Coastal Escarpment Model

A 1:50 scale model of the coastal escarpment located at Wind Energy Institute of Canada's wind farm in Prince Edward Island, was made from four large Expanded Polystyrene (EPS) blocks, which were cut using a FrogMill CNC machine, as per the land survey data provided by the Provincial Government of Prince Edward Island. The escarpment model was divided into three separate pieces, each of which consisted of two solid layers of EPS foam glued together (see Figure 3-1). The entire model was painted black with latex paint to provide smooth texture. The model was approximately 7 m wide, 0.28 m high and approximately 6 m long. Solid ramps constructed from EPS with slopes of roughly 45°

were used along the back of the model to assure a smooth transition and to prevent any flow separation. Additional masonite boards were fastened to model's edges in regions which were practically outside of the active flow zone. In addition, plasticine was used to fill in any local mismatches at the joints of individual model blocks.

As mentioned earlier, two inflow conditions; open-water ESDU boundary layer profile and sea breeze profile (measured at the site) were considered. For measurements using the ESDU inflow profile, the model was positioned at roughly 12.5 m from the 60-fan wall which coincides with the center of the turntable. Likewise, during measurement involving the sea-breeze profile, the model was placed at the edge of the turntable, 10.5 m from the 60-fan wall. The blockage ratio which is defined as the ratio of the model frontal area divided by the cross-sectional area of the test section was approximately 7%. Three wind directions 230°, 270°, and 300°, were investigated. Each of these wind directions comprised of unique local topographic features of the escarpment exposed to the incoming wind as shown in Figure 3-1. The topographic feature at 230° transect was a quasi-two-dimensional step, with a concave curvature (see Figure 3-1 bottom right). At 270° transect, an upstream peninsula was located which extended roughly 0.40 m (20 m full-scale) from the escarpment edge and raised from 0.12 m (6 m full-scale) to escarpment height (see Figure 3-1 middle). Along this wind direction, there was a gap between the peninsula tip and the escarpment edge. The escarpment profile at 300° transect was a near-triangular extrusion with a slightly upwind sloped edge and downwind loped plateau (<2°), see Figure 3-1 (bottom left). The location of wind turbine (80 m hub height and 93 m rotor diameter) at the actual site was also marked in Figure 3-1 (top). The chalk lines show the wind direction, centered at the wind turbine, which were used as reference to align the model with the incoming flow for each wind direction. Hereinafter, the three wind direction cases are referred to as WD230, WD270, WD300.

3.4　Velocity Measurements

The flow velocities were measured using Cobra Probes, developed by Turbulent Flow Instrumentation Pty Ltd. Cobra Probes are dynamic four-hole pressure probes used to measure all three components of the mean and fluctuating velocities as well as the static

pressure within a 45° cone of acceptance. The uncertainty of velocity measurements is ±0.5 m/s and the pitch and yaw angles have an uncertainty of ±1.0°. In the
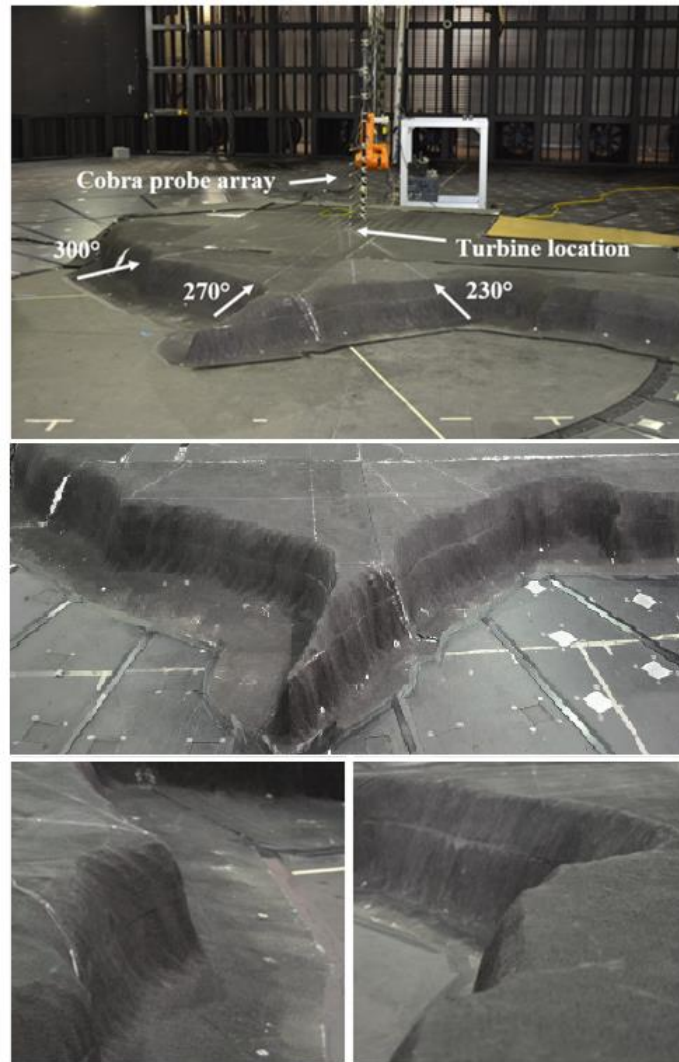
Figure 3-1: Scaled model of a section of the Research and Development Park, P.E.I. Shown are the three wind directions investigated with the rake of Cobra Probes at the turbine location (top), an above view of the escarpment geometries (middle) and views of the escarpment sections from 230° (bottom right) and 300° (bottom left)

present study, 10 Cobra Probes were used that were mounted on a carbon fiber mast as a vertical rake. The mast was attached to a robotic arm mounted on a traverse system which was mounted on rails attached to the ceiling of the wind chamber. During experiments, the rake was moved axially at 10 locations starting at the escarpment edge ($x/h = 0$ m) and up

to the turbine location ($x/h \approx 7.5$). The velocity measurements were sampled at 1250 Hz for 3 minutes at each axial position. A schematic of the rake can be seen in Figure 3-2. The total vertical distance covered by probes was from 0.06 m (3 m full-scale) to 1.6 m (80 m in full-scale), measured from the surface of the model. The top probe in the arrangement was positioned at the hub height of the turbine at the field site, while three probes were located within the lower radius of the turbine (33.5 m full-scale). Hereinafter, the three velocity components are referred to as streamwise (u), spanwise (v) and vertical (w).
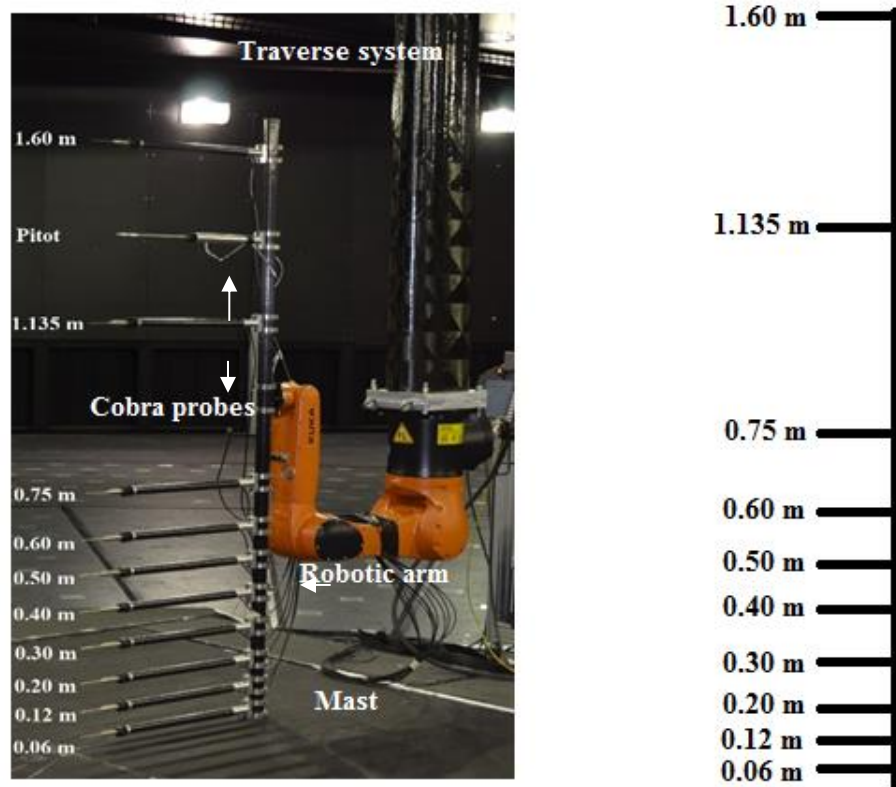
Figure 3-2: Cobra Probe rake (left) and depiction of the heights of Cobra Probes (right)

3.5 Data Processing

The Cobra Probes are not very effective in measuring velocities in regions of reverse flow. Therefore, regions of reverse flow can be identified through time series which contain a

large amount of poor quality data. In this case, the poor-quality data is defined as measurements which fall below the lowest acceptable velocity (2 m/s) in areas of flow separation. Spot checks of the time series was done prior to post processing and any time series that contained more than 20% poor quality data was removed from the subsequent analyses. The mean velocities (*U, V,* and *W*) were obtained by time-averaging the corresponding instantaneous velocities. The speed-up ratio, often used to describe the influence of the topography on the mean flow in relation to potential increases\decreases in wind energy and structural pressures, is computed as:

$$\Delta S = \frac{U(x,z)}{U_o(z)} \tag{3.1}$$

where $U(x,z)$ is the streamwise velocity at a height of z over the local terrain and $U_o(z)$ is the upstream mean velocity at the same height z. The upstream reference velocity profile was measured roughly at the edge of the escarpment in the absence of the model for each case and the boundary layer thickness across the test section (not shown here) was found to be constant. Turbulence intensity of each velocity component was computed by normalizing the root mean square of the fluctuating component by the mean streamwise velocity. The turbulent kinetic energy is defined as:

$$TKE = \frac{1}{2}\left(\overline{u'^2} + \overline{v'^2} + \overline{w'^2}\right) \tag{3.2}$$

where u', v', and w' are the fluctuation velocity components.

3.6   Inflow Profiles

As mentioned above, two inflow conditions were produced in this study; the first was a standard ESDU inflow profile for open water and the second was the actual sea-breeze profile measured in full-scale at the wind farm site. To create the desired inflow conditions, a wooden contraction was installed downstream of the 60-fan wall to increase the flow uniformity and velocity magnitudes across the test section. The ESDU profile was created by manipulating the 60-fan wall and setting the first row of fans to 50%, the second row to 60%, the third row to 60% and the fourth row to 70% of the maximum fan RPM and using the roughness elements in the chamber set to a height of roughly 10.5 cm. For the sea-

breeze profile, many iterations of inflow conditioning were conducted, using a combination of sheared vertical flow by manipulation of the 60-fan wall within the WindEEE dome, roughness elements, spires and different sized trips. The best match to the full-scale sea breeze profile was obtained using a configuration of fans which consisted of the first row at 80%, the second row at 65%, the third row at 71% and the fourth row at 30% of the maximum RPM as well as a wooden trip section 10.4 cm high, installed near the end of the contraction exit, spanning from wall to wall. A rake of 11 Cobra Probes arranged in a similar set as described above was used to measure the inflow velocities at the model site (in the absence of the model). Figure 3-3 shows the mean velocity profiles for both inflow conditions. The standard ESDU profile (Figure 3-3a) and the field-measured sea breeze profile (Figure 3-3b) are also plotted for comparison.

Figure 3-3a shows the comparison of the open-water boundary layer flow produced in WindEEE dome with that of the ESDU standard. Both the mean velocity and turbulence intensity are in good agreement. However, there is a slight increase in mean velocity and consequently a decrease in turbulent intensity between a height of 15-25 m full-scale. Overall, the differences between the generated and standard ESDU mean velocity and turbulent intensity profiles were 5% and 14%, respectively, indicating that the ESDU boundary layer profile was physically produced with good accuracy.

The inflow Reynolds number in the present study for the ESDU profile, based on hill height, h, and mean upstream velocity at hill height, U_h, was equal to $Re_h = 3.1 \times 10^5$. The friction velocity, u_*, and the roughness length, z_o, were estimated by fitting the profile of mean streamwise velocity in the logarithmic region to the standard logarithmic wind profile for a neutrally stratified atmospheric boundary layer given as [25],

$$U(z) = \frac{u_*}{k} \ln(\frac{z}{z_o}) \tag{3.3}$$

where $U(z)$ is the mean streamwise velocity at height z, k is the Von Karman constant equal to 0.41, u_* is the friction velocity, and z_o is the roughness length. The data fitting provided friction velocity and roughness length of $u_* = 0.586$ m/s and $z_o = 0.0003$ m,

respectively. The roughness length associated with this boundary layer flow is in good agreement with that reported in the literature for the open sea [26].

Figure 3-3b shows the comparison between the full-scale sea-breeze mean wind velocity profile measured over a period of roughly one hour with a scanning lidar [27] and measurements in the WindEEE dome. The hill height Reynolds number of the sea-breeze profile was $Re_h = 2.65{\times}10^5$. The results show a reasonable agreement between
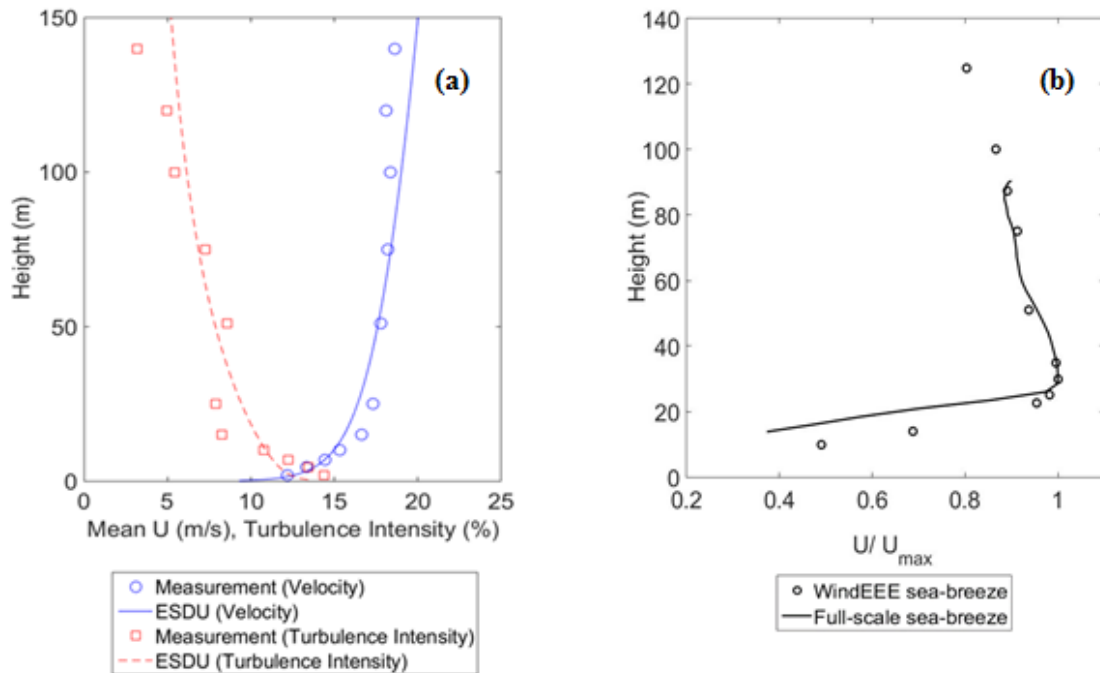
Figure 3-3: Inflow profiles of boundary layer flow compared to ESDU (a) and sea breeze inflow profile compared full-scale (b)

the two profiles with an overall difference of 5%. There is some discrepancy in the velocity profiles below hill height (close to 20%), which arose due to the challenges in producing high shear near the surface as per the field-measured profile. This was achieved by creating an upstream shear layer in the near surface region that increased inertia and due to the presence of the trip section, consequently, resulted in high magnitudes of near-surface turbulence. Near surface turbulence intensities (not shown here) reach levels exceeding 40% closest to the surface and did not behave as typical atmospheric flow. The turbulence

levels reduced to typical levels of roughly 8-10% from 25 m < Z < 50 before increasing again to 20% Although the model was placed in the far wake of the trip section (greater than 10 times the trip section height), it is believed that the large-scale structures shed from this trip section did not properly diffuse before interacting with the model. Unfortunately, due to time constraints, the authors did not have an opportunity to further condition the flow to properly match turbulence characteristics. This exercise highlighted the challenges in properly simulating the structure of both mean and turbulent flows when the upstream conditions are different from the classical cases. Furthermore, it indicates that the matching of mean velocity profiles does not guarantee the matching of turbulent behavior.

As the physically simulated inflow profile for open-water ESDU case matched well with the classical profiles for both mean and turbulent flows, the detailed flow characteristics over the escarpment are presented for this case in the subsequent sections. For the sea breeze inflow case, the physically simulated mean profile matched with that from the field but the turbulent velocity magnitudes were not realistic. Hence, in the subsequent section, only the mean flow characterization over the escarpment subjected to sea breeze conditions are presented.

3.7   Influence of Inflow Profiles on the Mean Flow Field

3.7.1 ESDU Inflow

The normalized mean velocity profiles over the escarpment due to the open-water ESDU inflow conditions are presented in Figure 3-4 for all three wind directions. The results show that WD230 and WD300 wind directions that are subjected to slightly concave and pointed topographic profiles, have similar mean flow behavior past the leading edge of the escarpment for all three velocity components. Further downstream, differences are observed in the streamwise and vertical mean velocity components. At WD230 the streamwise velocity shows some local deceleration along with a decrease in the spanwise velocity magnitudes. The results also show that the wake region for WD230 case started to grow faster for $x/h > 1$ resulting in a wake almost twice as high as that of WD300 at the turbine location of $x/h = 7.5$. These trends are likely due to the differences in the small-scale features of the escarpment edge in each test case. The edge of the escarpment of
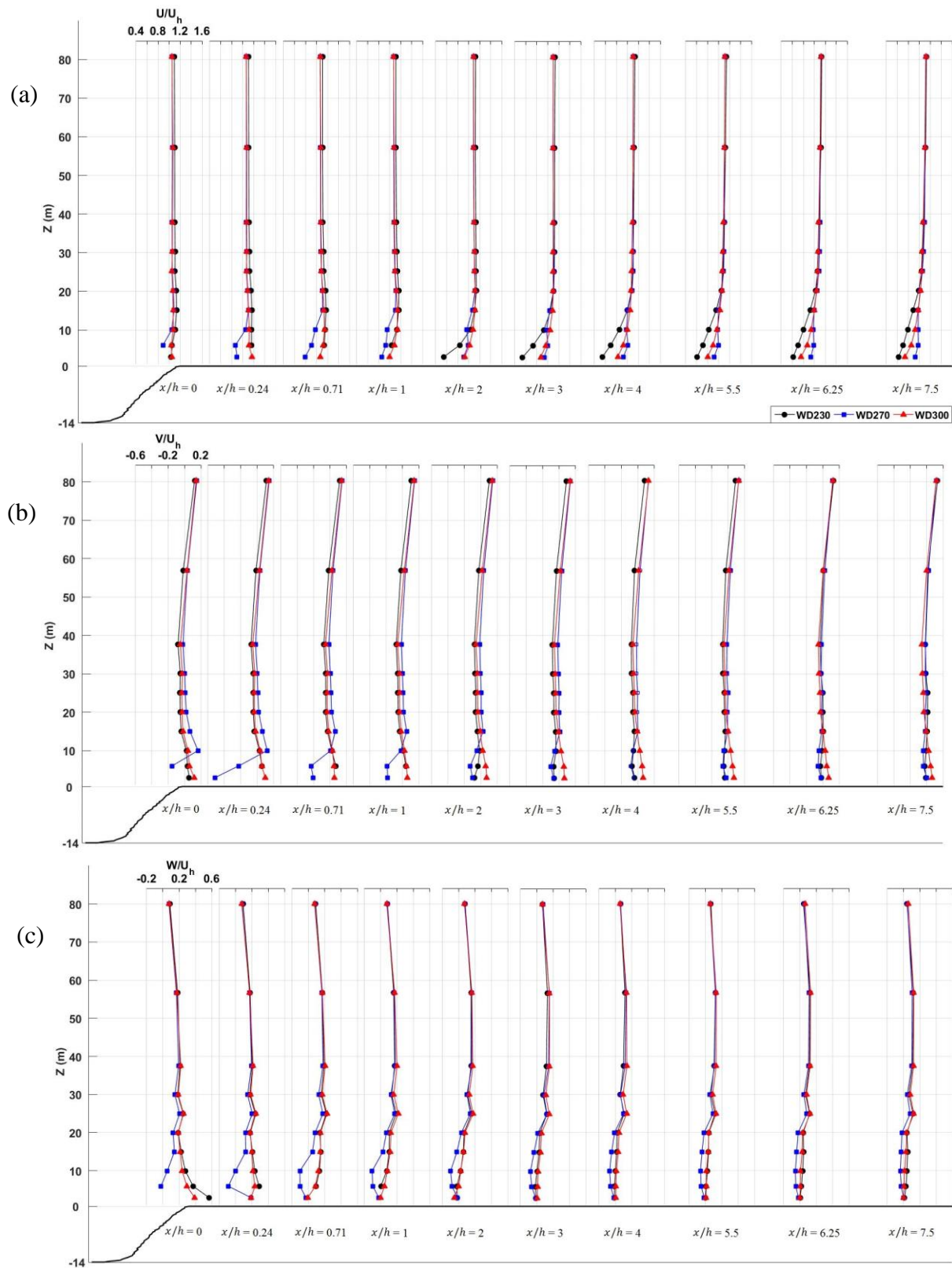
Figure 3-4: ESDU inflow vertical profiles of U (a), V (b), and W (c) normalized by velocity at hill height. Legend of (a) applied to all figures and the scale of x/h = 0 applies to all plots. Turbine location is at x/h = 7.5.

WD230 has a sharper transition versus the pointed, upwind sloped edge of WD300 which provides a smoother transition over the step.

The mean velocity behavior of WD270 is significantly different from the other two wind direction cases. The case of WD270 shows that the flow interacted with the peninsula which extends upstream approximately x/h = -1.43 from the escarpment edge, and significantly affected the flow downstream. This topographic pattern created large gradients in the span wise and vertical direction, which produces a seemingly two-layer flow. A small separation bubble formed downstream of the escarpment leading edge that extended up to a height of approximately 10 m above the surface. The results also indicate that the reattachment point is located between $0.71 < x/h < 1$. Results also show a local acceleration in the streamwise flow which reduced the wake region at the turbine location compared to the other wind direction cases.

The results in Figure 3-4 show that the local topographic pattern can influence all three velocity components of the flow over the escarpment. Depending on the topographic pattern, the influence can be more significant in the vicinity of the leading edge or further downstream. It is however observed that, their influence is mainly restricted to the near-surface region $Z < 20$ m.

3.7.2 Sea Breeze Inflow

Figure 3-5 shows the normalized velocity profiles for all three wind directions for the sea-breeze inflow condition. When sea-breeze inflow conditions are used WD270 and WD300 show almost identical behavior downstream of the escarpment edge for all three velocity components despite having vastly different topographic patterns. The streamwise velocity profiles (Figure 3-5a) indicate that for all three wind directions, a high shear region forms at the leading edge of the escarpment within 10 m above the surface, which started to extend with the downstream distance and reached up to a height of 20 m at the turbine location. WD230 case showed different behavior than the others in this region with lower magnitudes and almost linear variation.

The spanwise velocity was found to be negative just above the surface at $Z = 3$m for the
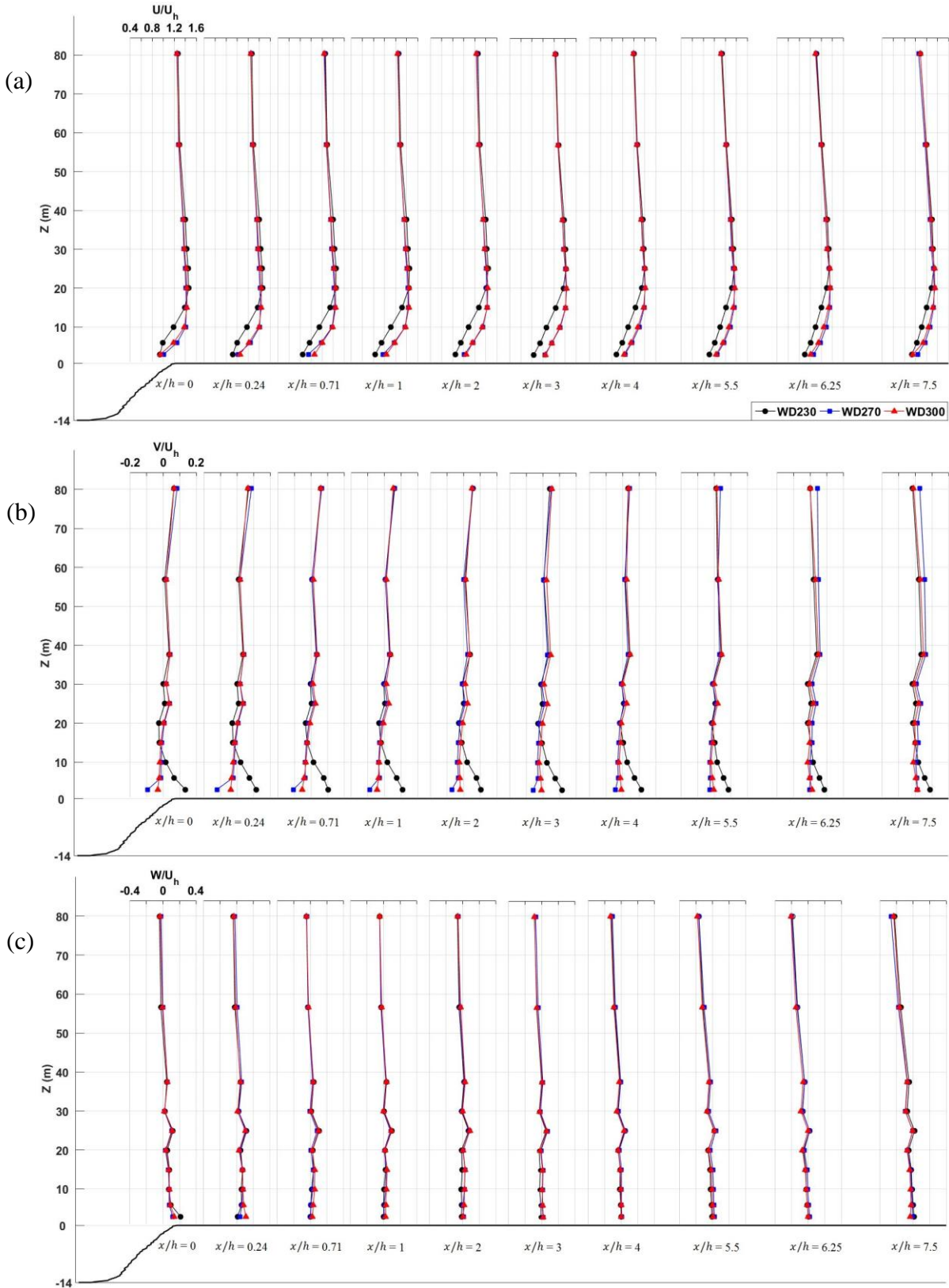
Figure 3-5: Sea breeze inflow vertical profiles of U (a), V (b), and W (c) normalized by velocity at hill height. Legend of (a) applied to all figures and the scale of $x/h = 0$ applies to all plots. Turbine location is at $x/h = 7.5$.

WD270 and WD300 cases and gradually became positive with an increase in height (see Figure 3-5b). The negative spanwise velocity magnitude for WD270 case was higher than that for the WD300 case. Negative spanwise velocities indicate that the flow diverges from the wind direction transect. The shape of the geometries is assumed to be the cause for this divergence as the peninsula is curved in such a way that the separation would not be along the straight transect line as shown in Figure 3-1. The same is true for WD300, where the triangular shape of the escarpment would act as a wedge to diverge the flow away from the transect line. As the flow moved further downstream, the spanwise velocity magnitude decreased and became almost zero at the turbine location. The spanwise velocity for WD230 cased showed a different trend in the shear region identified in Figure 3-5a. A large spanwise velocity magnitude exists near the surface, which decreased towards the upper edge of the shear region and with an increase in the axial distance. This high magnitude of spanwise velocity for WD230 case is linked with the lower streamwise velocity through mass conservation. This behavior is most likely due to the channeling effects from the escarpment section caused by the long coastline to the right of Figure 3-1 (top). The vertical velocity profiles (Figure 3-5c) show that the vertical velocity is almost zero in the near-surface region and gradually becomes negative with a further increase in height. The results are similar for all three wind direction cases.

The results in Figure 3-5 indicate that for sea-breeze inflow condition, the most complex topographic feature i.e. the case of WD270 did not create a unique flow structure. Additionally, the sea-breeze profile did not develop into a boundary layer over the extent of the model, but the behavior of the flow beneath 20 m indicates that a high shear region is present. Field measurements of sea-breezes have shown that it is not uncommon for the fronts to penetrate modest distances inland (hundreds of metres) in the least ideal conditions [28]. Therefore, it is not unreasonable to assume that given a longer fetch, a shear region would have developed on the model.

3.7.3 Comparison to Full-scale Data

The field study at the real escarpment not only measured the inflow sea breeze profile but also measured the velocity profile over the escarpment at three axial locations. In order to further assess whether the sea breeze inflow reproduced in the WindEEE captured the real

flow behavior as it passes over the escarpment, another set of experiments were conducted. The scanning lidar used to measure the sea-breeze inflow in the field also measured velocity profiles at distances of $x/h = 0$, $x/h = 0.36$ and $x/h = 0.71$ measured from the escarpment edge along the 262° axis. To match the conditions of full-scale, the model was oriented in the WD230 configuration while Cobra Probe rake was aligned along the 262° to match the line of sight of the lidar during the full-scale measurements. The 262° axis is visible in Figure 3-1 between WD230 and WD270.

Figure 3-6 shows the comparison between full-scale velocity profile measurements and the current study using both inflow conditions at positions corresponding to the above full-scale locations.
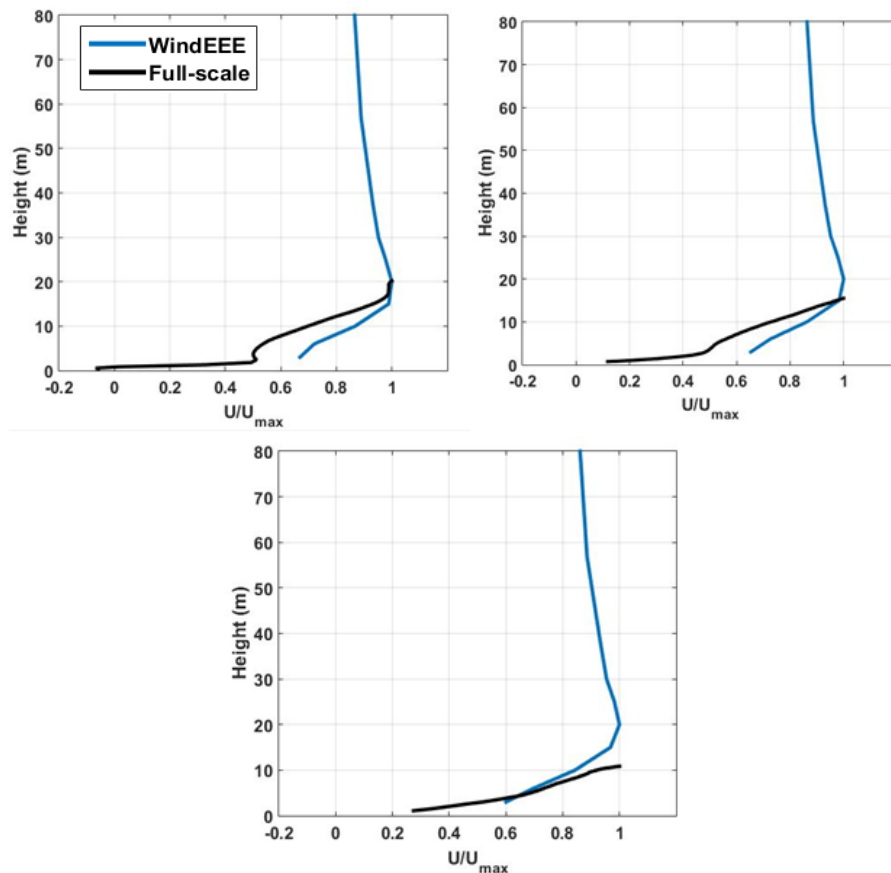

Figure 3-6: Horizontal velocity normalized by the maximum velocity of the WindEEE study compared to full-scale lidar measurements at $x/h = 0$ (a), $x/h = 0.36$ (b) and $x/h = 0.71$ (c). Legend in (a) applied to all plots.

The results indicate that at $x/h = 0$ and $x/h = 0.36$, the measured velocity profiles over the scaled model under sea breeze conditions have trends similar to that of full-scale data but the normalized magnitudes are overpredicted. There is an overall difference of roughly 17% in WindEEE and full-scale velocities. At $x/h = 0.71$, the WindEEE velocity magnitudes are underpredicted with an overall difference of about 14%. These results indicate that the mean flow field in the near escarpment region under sea breeze inflow conditions is reproduced reasonably well in the WindEEE. One plausible explanation for the differences are the limitation of scaled modelling in properly resolving small-scale features, particularly at the escarpment edge. It has been shown in a recent study by Kilpatrick [29] that small changes to features of an escarpment edge can lead to significant changes to the mean and turbulent structure of the downstream flow field.

Further comparison of the flow field can be made by comparing the hub height velocity in WindEEE at the turbine location ($x/h = 7.5$) to the actual hub height wind speeds measured atop the turbine during the sea-breeze conditions. A majority of wind tunnel testing with respect to wind energy and wind resource assessment assesses topography in the absence of a wind turbine. This study is unique in the sense that the hub height wind speeds at the turbine location can be validated by hub height anemometer data during the period when the full-scale sea-breeze inflow was measured. Table 3-1 presents the normalized hub height wind speeds (U) at the turbine location from lab and field data under sea breeze conditions. The point of maximum velocity is also presented for comparison. The results show very good agreement between the lab and field data for both hub height and peak velocities with differences of 4% and 3%, respectively.

Table 3-1: Comparison of normalized hub height horizontal velocity at the turbine location

	Boundary layer	Sea-breeze	Full-scale
$U_{hub}/U_{inflow\ 30}$	1.082	0.75	0.792
$U_{hub}/U_{inflow\ 80}$	1.027	0.855	0.885

3.8   Effect of Local Topography on the Mean Flow Field

The mean flow behavior of the three velocity components under ESDU conditions have already been presented in Section 3.7. To further investigate the impact of the local escarpment topography, the two-dimensional streamlines based streamwise and vertical velocity components are presented in Figure 3-7 for the three wind direction cases. The streamlines for WD230 and WD300 cases are very similar over the entire flow field above $Z = 6$ m showing a divergence of streamlines around $Z = 20$ m. The streamlines of WD270 show larger divergence near the surface compared to the other cases. The convergence of the streamlines below $Z = 10$ m depicts the acceleration shown in the mean flow.
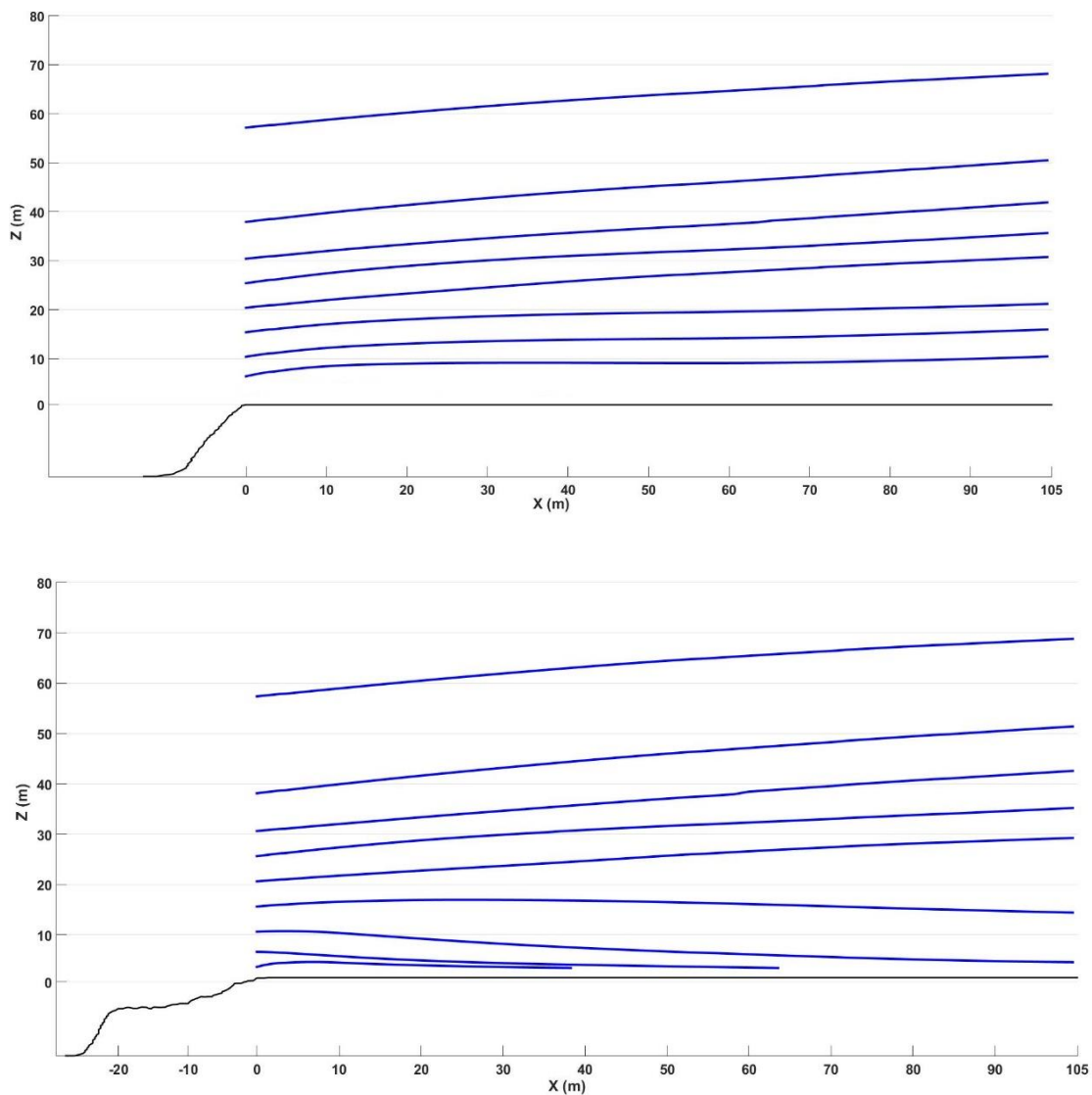
Figure 3-7: streamline plots for WD230 (a), WD270 (b) and WD300 (c) on the respective escarpment profiles.

The streamlines for WD230 and WD300 cases are very similar over the entire flow field above $Z = 6$ m showing a divergence of streamlines around $Z = 20$ m. The streamlines of WD270 show larger divergence near the surface compared to the other cases. The convergence of the streamlines below $Z = 10$ m depicts the acceleration downstream shown in the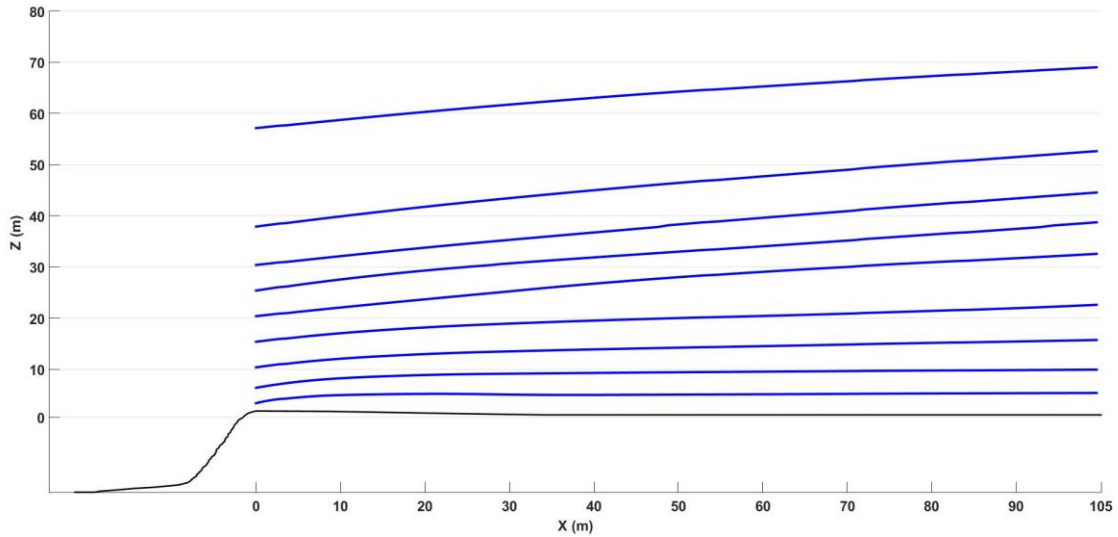 mean streamwise component in Figure 3-4a. Flow visualization was also conducted for the case of WD230, shown in Figure 3-8, which revealed features of the flow which
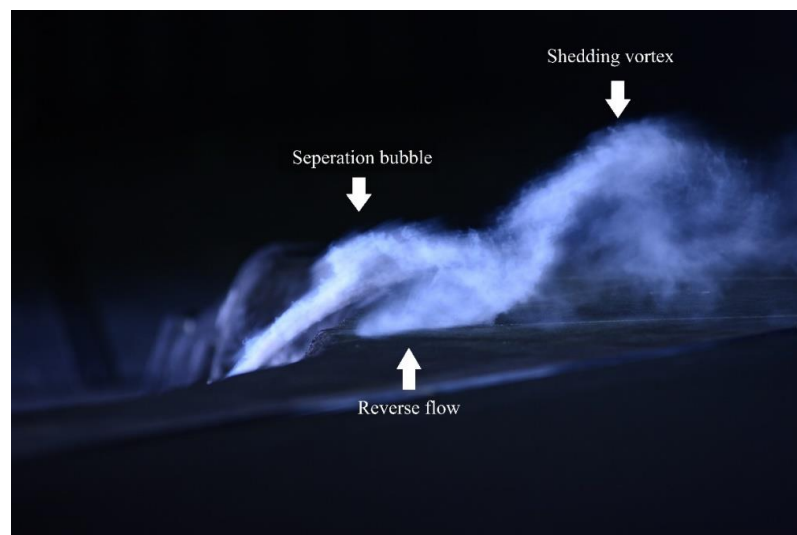

Figure 3-8: Flow visualization downstream of the escarpment for WD230.

were not able to be captured by the Cobra Probes. Three distinct features can be seen near the surface downstream of the escarpment. The shear layer and separation bubble can be seen with a small region of reverse flow near Z = 3 m. Additionally, a secondary vortex can be seen leaving the separation bubble and travelling downstream.

In engineering applications, it is often useful to know to what extend the flow is modified by the terrain to determine placement of structures from topographic features. For structural applications, wind induced pressures are proportional to the squared wind speed while for wind energy applications, the power output is proportional to the cubed wind speed. To provide a better sense of the influence of the topographic features on the extend of the flow modification compared to the upstream, the speed-up ratios are plotted in Figure 3-9. Also, plotted in Figure 3-9 is the speed-up ratio as defined by the National Building Code of Canada (NBCC) given as [30]:

$$\Delta S = \Delta S_{max}\left(1 - \frac{|x|}{kL_h}\right)e^{-\frac{\alpha z}{L_h}} + 1 \tag{3.4}$$

where ΔS_{max} is $1.3h/L_h$ for a two-dimensional escarpment, x is the horizontal distance upstream or downstream of the escarpment crest, L_h is the horizontal distance upstream from the crest of the escarpment to the point where the surface is half the height of the feature, z is the height above local ground, $\alpha = 2.5$ for 2-D escarpments and k=4 for $x \geq$ 030). The cases of WD230 and WD300 can be assumed to be quasi-two dimensional features, thus the comparison to the NBCC is not unreasonable. This same assumption is not valid for WD270 and thus the comparison to the NBCC should be taken with some skepticism.

The speed-up ratio for the WD 230 and WD300 showed very similar behavior to the NBCC within one hill height downstream, except for the escarpment edge where the NBCC overpredicted by roughly 13% in both cases. In the case of WD300, there was reasonable agreement for most of the axial measurement length, where the best comparison was within one hill height downstream. In the case of WD230, the separation region and downstream wake formation as shown through the mean velocity profiles and visualization led to the overprediction by the NBCC. Bitsuamlak et al. [31] noted that there are discrepancies in

results of flow over a hill between wind tunnel, CFD, analytical and NBCC at the hilltop when a steep hill is used, likely indicating that separation is the cause for this difference. It was also shown that the terrain roughness plays a significant role in the onset and leeside characteristics of separation, with roughness increasing the extent of the separated region.
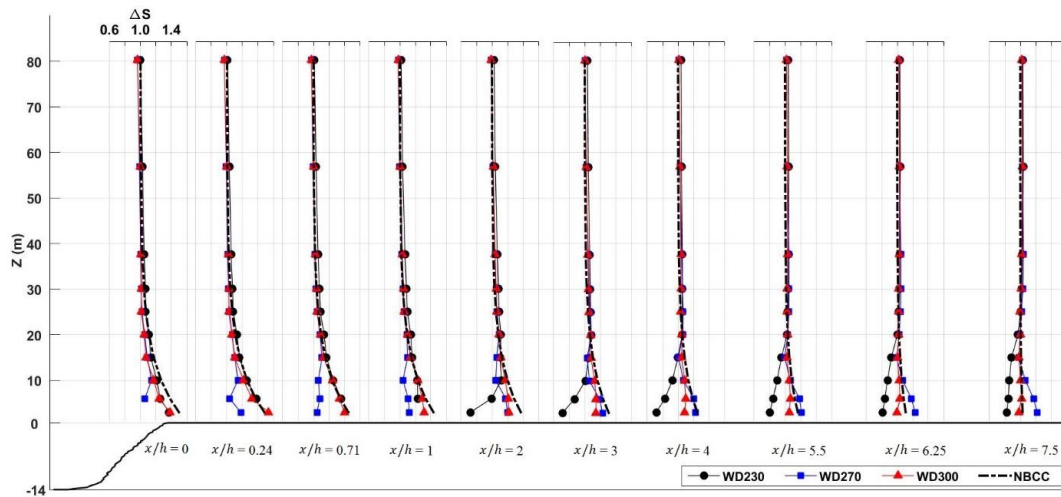
Figure 3-9: Vertical profiles of speed-up ratio compared to the National Building Code of Canada guidelines for a two-dimensional escarpment. Turbine location is at $x/h = 7.5$.

This explains the error at the edge of the escarpment for WD230. The wake downstream of WD230 had a much larger effect downstream to the turbine location showing large differences between the NBCC and the present study.

The upstream peninsula in the WD270 case creates two regions of significant speeds-up just downstream of the escarpment. At $x/h = 0.24$ two local speed up regions exists separated by a layer not affected by the local topography showing virtually no speed-up. An increase in velocity compared to the upstream of 17% can be seen at heights of $Z = 3$ m and $Z = 10$ m at this location. A short distance downstream at $x/h = 0.71$, the near surface region experiences a velocity reduction in the wake before beginning to accelerate at $x/h = 3$ reaching a speed-up of $\Delta S = 1.2$ which is almost constant to the turbine location. Meanwhile, at $x/h = 0.71$, the region just above at $Z = 10$ m remains relatively unchanged to the turbine location. The overprediction of the speed-up ratio from $0 < x/h < 3$ is most

likely attributed to the separation and wake at this wind direction, while the flow acceleration leads to an underprediction at the turbine location.

3.9   Effect of Topography on the Turbulent Flow Field

3.9.1   Turbulence Intensity and TKE

As previously stated, the turbulent field will only be analyzed for the ESDU inflow case, due to issues in accurately simulating inflow turbulence intensities in the sea breeze case. The turbulence intensity of each wind direction is separated into the individual velocity components in Figure 3-10. Generally speaking, all of the velocity components for each of the examined cases are very similar. Minor differences below $Z = 10$ indicating slight anisotropy near the surface. Within one hill height from the escarpment edge, WD230 and WD300 show very similar levels of turbulence intensities above $Z = 3$m. The maximum turbulence intensity of WD230 can be seen at the location of the largest velocity deficits in the streamwise component (see Figure 3-4a) at $x/h = 2$ corresponding to the growth of the wake. Further downstream, as the wake begins to grow, the turbulence intensities in the streamwise and vertical direction increase with both height and distance downstream whereas the spanwise intensity remains roughly constant from $5.5 < x/h < 7.5$. This is indicative of the vertical mixing of the wake downstream. The cases WD230 and WD300 are dissimilar for $x/h > 1$, where there the turbulence intensity remains relatively unchanged outside of the small increase in σ_u at $Z = 3$m typical of wall-bounded flow. At the turbine location, the results show that WD230 has the highest intensity in all three components up to a height of $Z = 20$m.

As expected, WD270 shows much different behavior in the turbulence intensity. The turbulent fluctuations are the most intense in all directions for this case up to $x/h = 1$ and shows much more rapid wake formation compared to the other two wind directions. The streamwise profile along WD270 reveals that the profile is similar from $0 \leq x/h \leq 0.24$ and increases at $x/h = 0.71$ above and below $Z = 6$ m. Maximum intensities of roughly 33% are achieved at $Z = 3$ m from the surface at this point and decrease downstream and the flow accelerates to the turbine location. Atop the accelerated region, the wake above the shear layer formed due to the peninsula broadens downstream and
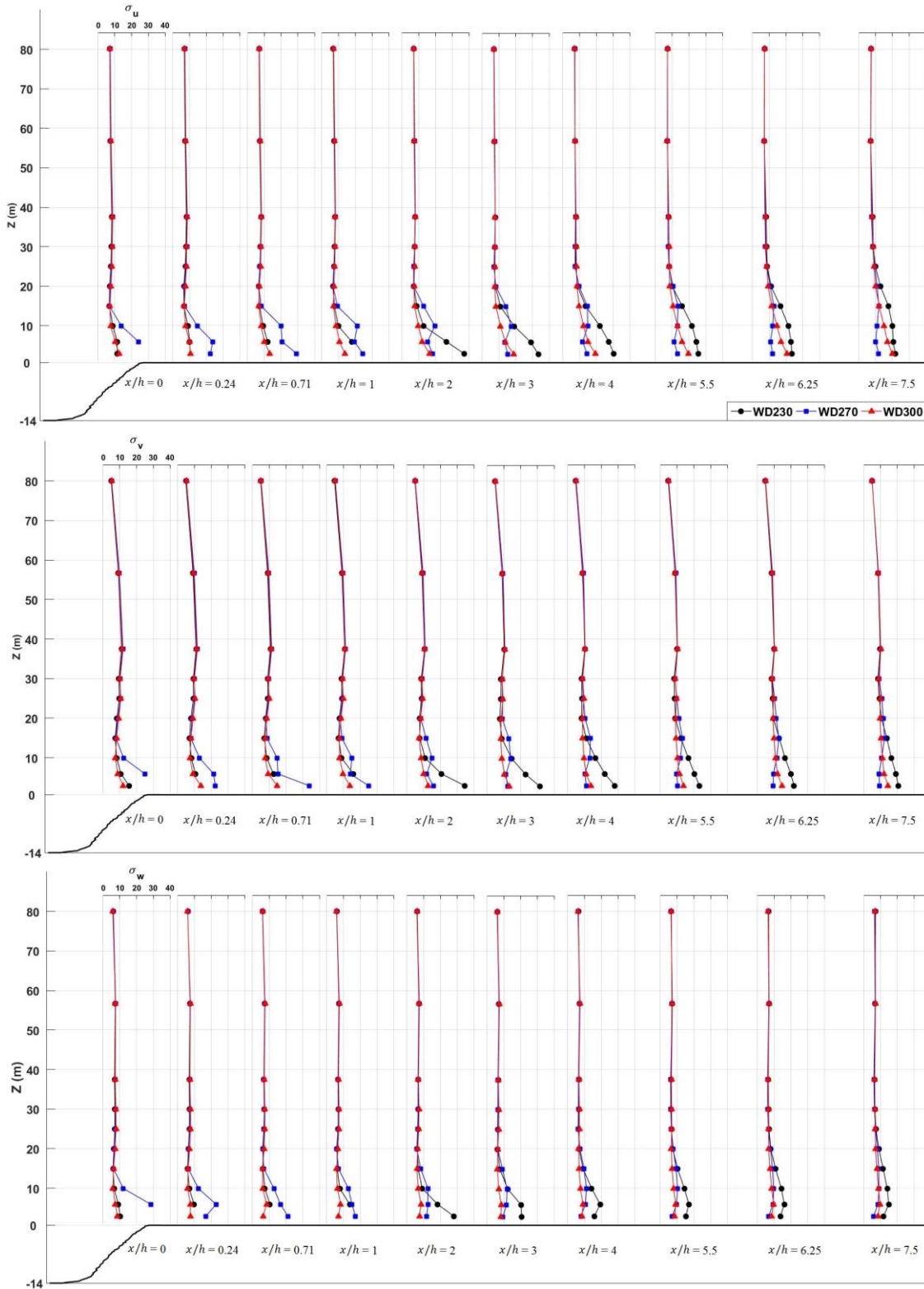
Figure 3-10: Turbulence intensity, in percentage, of U (a), V (b) W (c). Legend in (a) applies to all figures and scale of $x/h = 0$ applies to all plots. Turbine location is at $x/h = 7.5$.

increases in height to $x/h = 3$ showing effects up to $Z = 30$ m at the turbine location. In the spanwise direction, the intensity increased downstream of the leading edge and becomes the largest of the three components at $x/h = 0.71$ as the magnitude of the spanwise velocity decreases (Figure 3-4b). A similar trend to the streamwise component is observed downstream. The vertical component has the smallest values of all three components and the results reveal that a relatively large value of turbulence intensity is present at the leading edge due to the almost zero vertical velocity at $Z = 6$ m. An increase near the surface is present in line with the other two components and the overall profile broadens downstream.

Similar trends to the turbulence intensity can be seen in the TKE profiles in Figure 3-11. The results indicate similar behavior in the TKE for the cases of WD230 and WD300 from $0 < x/h < 0.71$. Further downstream at $x/h \geq 1$, the TKE for WD230 case increased relative to the WD300 case, which is likely caused by the increased perturbations present in the wake of the separated region after reattachment. This high TKE region reduces and broadens downstream to the turbine location where the increased turbulence is still present.

Figure 3-11: Vertical profiles of TKE normalized by the squared hill height velocity. Scale of $x/h = 0$ applied for all plots. Turbine location is at $x/h = 7.5$.

The highly turbulent region at the leading edge of the escarpment caused by the upstream peninsula in the case of WD270 shows a local maximum at $Z = 10$ m which propagates downstream, but to a lesser extent compared to the wake created from WD230. The strong

turbulence observed initially downstream of the escarpment edge are reduced near the surface while a wake profile is observed. In the accelerated region below $Z = 6$m, the magnitudes of TKE are reduced as the flow becomes less turbulent. Moving downstream, the wake begins to broaden covering a wider range compared to the other two cases range from 6 m $< Z < 30$ m at the turbine location.

3.9.2 Reynolds Stress

To gain more insight into the wake behavior downstream, the Reynolds shear stress is plotted for each case in Figure 3-12. The Reynolds shear stress, indicative of the streamwise momentum flux in the wall normal direction, implies there is a greater amount of mixing downstream of the leading edge where there are large magnitudes of $-\overline{u'w'}$. In the canonical case of a forward-facing step, this increased mixing is the driving factor in promoting the reattachment of a separated shear layer by pulling high momentum fluid towards the surface [32]. For each case, the enhanced Reynolds stress can be seen within
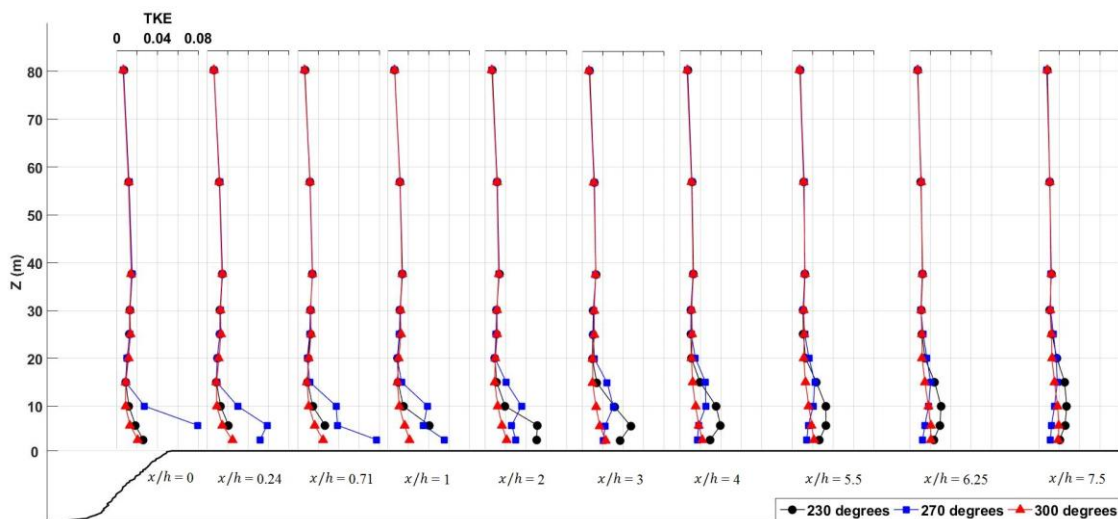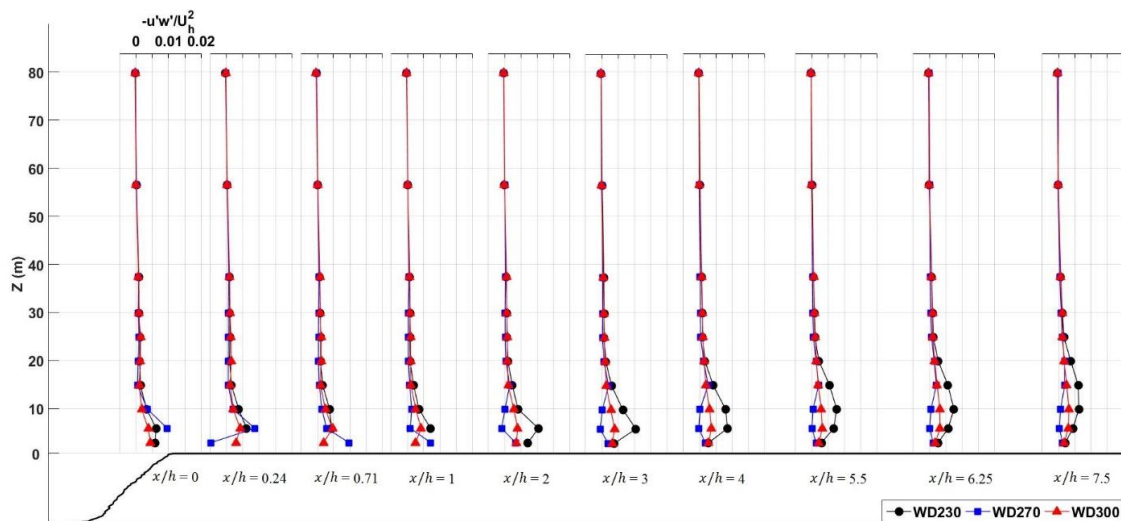

Figure 3-12: Vertical profiles of Reynolds shear stress normalized by squared hill height velocity. Scale of $x/h = 0$ applied to all plots. Turbine location is at $x/h = 7.5$.

10 m from the surface near the leading edge of the escarpment. In the case of WD230, the Reynolds stress magnitude started to increase beyond $x/h =1$ reaching a maximum at x/h $= 2$ at $Z = 6$ m. The point of the maximum shear stress is often observed above the shear

layer and downstream from the reattachment point and has been shown in the studies by Sherry et al. [32] and Kilpatrick et al. [29] for flow over a forward-facing step and flow over an escarpment with Reynolds numbers of $Re_h = 6741$ and $1.7{\times}10^5 < Re_h < 5.21{\times}10^5$ respectively. In this case, it is not unreasonable to assume that the separation bubble observed from the flow visualization reattaches somewhere between $1 < x/h < 2$. The peak Reynolds shear stress of 0.01 is in good agreement with the results presented in Kilpatrick et al. for the flow over a similar escarpment with a rounded edge. Downstream of this inferred reattachment point, the shear stress profile flattens and spreads due to the turbulent mixing in the wake and reaches a height of 20 m at the turbine location. Among the three wind direction cases, WD300 has the lowest magnitudes of Reynolds stress. The complex geometry on the peninsula for the WD270 case creates positive values of Reynolds shear stress at $x/h = 0.24$. which is likely caused by the flow separating just downstream of the escarpment edge. Positive Reynolds shear stress is often associated with increased wall normal velocity, which are present in Figure 3-4c, and acts to move the lower momentum fluid upwards to the outer flow. A short distance downstream the shear stress reaches its maximum at the onset of flow acceleration after reattachment at $x/h = 0.71$. The shear stress becomes negative 3 m above the surface at $x/h = 0.71$ m where it reaches its minimum indicating momentum transfer away from the wall and slightly increases with increasing axial distance and is stays roughly constant above $Z = 3$ m from $1 < x/h < 7.5$.

3.10 Discussion

The results of the investigation of the flow field over the escarpment from different wind directions, which have different local topography, indicate that the extend of the flow modification is confined to 20 m ($1.5h$) above the surface. Therefore, the wind turbine downstream at $x/h = 7.5$ does not seem to be positively or negatively affected, in terms of power production as the lower radius of the turbine rotor reaches 33.5 m from the surface. However, it is speculated that further propagation of the effects of the local topography downstream may affect other wind turbines on the site as there are parallel wind turbines from the wind directions of 230° and 300°.

Although the wing turbine blades do not experience effects from the local topography, the location of the turbine is not far enough downstream to be unaffected in terms of structural loading issues on the tower. As wind induced pressures are proportional to the square of the wind speed, knowledge of the flow characteristics at the base of the tower are important for design considerations. In this case, if the NBCC code is used to determine the effects of the escarpment at the turbine location there may be some over/underestimation of design conditions. The highly turbulent, separated flow from 230° leads to a large overestimation in terms of design wind speed and hence the wind induced pressures. Increased turbulence intensity experienced at the base may cause increased fatigue loading and influence the dynamic response of the structure. From a wind direction of 300°, the wind induced pressures may be underestimated potentially causing underestimation of wind induced pressures. As the wind changes direction between 230° to 300°, the wind turbine structure could potentially see a series of these flow characteristics over a short time span.

3.11 Conclusions

An experimental study was conducted to physically simulate the flow over a 1:50 scale model coastal escarpment under both ABL and sea breeze inflows. The experiment is based on a previously documented full-scale campaign conducted at the Wind Energy Institute of Canada's Research and Development park in North Cape, P.E.I which houses five 2 MW wind turbines. The full-scale campaign investigated the flow over the escarpment in which measurements at multiple distances from the escarpment were taken using a scanning lidar. In the model scale experiment a set of Cobra Probes were used to measure all three velocity components from just above the surface to the scaled hub height ($Z = 80$ m) near the escarpment edge and extending back to the turbine location (105 m from the escarpment). The effects of the escarpment geometry were investigated by examining the flow field from 230°, 270° and 300° (from 0° North) which each have very different local topographic features.

Results between the comparison of the inflow conditions on the flow field show that the mean flow field is in better agreement with full-scale data when the proper inflow velocity profile is used. The normalized hub height wind speeds were in good agreement, showing a deviation from the actual wind speeds by 4% using the simulated sea-breeze inflow, while

considering a typical boundary layer inflow lead to an overestimation of roughly 30%. This highlights the importance of fully understanding the inflow profile and stability conditions when both physically and numerical modeling for the purposes of wind resource assessment.

The effect of small variations in topography was shown in the results using boundary layer inflow conditions typical of a coastal environment, as essentially two variations of an escarpment have two different effects on the flow downstream. A convex, pointed escarpment having an upwind sloped edge with a slight downstream slope almost entirely suppressed any separation with shedding vortices or wake from forming downstream. On the other hand, a slightly concave escarpment with a flat surface and slightly sharper edge created a small region of separation and a large wake downstream, reaching the local turbine sitting roughly 105 metres away from the edge. Thus, small features, such as sloping terrain and curvature of the step, have a significant impact of the mean and turbulent flow behavior downstream more than 7.5 hill heights. A more complex peninsula upstream of the escarpment created a shear layer much above the surface which propagated downstream in the form of a vertically displaced wake. Additionally, the flow accelerated downstream to the turbine location as the turbulence intensity and shear stress decreased underneath the wake. Overall, the effect of the escarpment geometry did not have an effect within the lower rotor radius, neither inhibiting or contributing to the wind turbine power or loading.

The WindEEE Dome at the University of Western Ontario proved to be instrumental in simulating inflows departing from typical neutral ABL flows as well as providing large scale simulations which allowed the detailed definition of the escarpment topography. The data from this study can be used to better calibrate linearized models which tend to be inaccurate for these combinations of inflows and topography.

References

[1] Palma, J. M. L. M., Castro, F.A., Ribeiro, L.F., Rodrigues, A.H., and Pinto, A.P., 2008. Linear and nonlinear models in wind resource assessment and wind turbine micro-

siting in complex terrain. Journal of Wind Engineering and Industrial Aerodynamics 96, 2308–2326.

[2] Walmsley, J.L., and Taylor P.A., 1996. Boundary-layer flow over topography: impacts of the Askervein study. Boundary-Layer Meteorology, 78, 291–320.

[3] Botta, G., Cavaliere, M., Viani, S., and Pospisil, S., 1998. Effects of hostile terrains on wind turbine performances and loads: The Acqua Spruzza experience. Journal of Wind Engineering and Industrial Aerodynamics, 74-76, 419-431.

[4] Rowcroft, J., Burton D., Blackburn H.M., Sheridan J., 2016. Siting wind turbines near cliffs – the effect of wind direction. Journal of Wind Energy, 19, 1469-1486.

[5] Bowen. A.J., Lindley D., 1977. A wind tunnel investigation of the wind speed and turbulence characteristics close to the ground over various shaped escarpments. Boundary Layer Meterology, 12,259–271. DOI: 10.1007/BF00121466.

 [5] Barthelmie, R.J., Palutikof, J.P.., 1996. Coastal Wind Speed Modelling for Wind Energy Applications. Journal of Wind Engineering and Industrial Aerodynamics 62.2-3 (1996): 213-36. Web.

[6] Burton, T., Sharpe, D., Jenkins, N., Bossanyi, E., 2001. Wind Energy Handbook. John Wiley & Sons.

[7] Wagner, R., Courtney, M., Gottschall, J., Lindelow-Marsden, P., 2011 Accounting for the speed shear in wind turbine power performance measurement. Wind Energy., 14, 993–1004

[8] Berg, J., Mann, J., Bechmann, A. Courtney, M.S., and Jørgenson, H.E., 2011. The Bolund experiment, part I: flow over a steep, three-dimensional hill. Boundary-Layer Meteorology, 141:219–243.

[9] Ayotte, K.W., 2008. Computational modelling for wind energy assessment. Journal of Wind Engineering and Industrial Aerodynamics 96, 1571–1590.

[10] Ayotte K.W., Sullivan P.P., and Patton E.G., 2010. LES and wind tunnel modelling over hills varying steepness and roughness. Fifth International Symposium on Computational Wind Engineering (CWE2010), May 23–27, Chapel Hill, North Carolina, USA.

[11] Petersen, E.L.,Mortensen, N.G., Landberg, L., Højstrup, J., and Helmut F.P., 1998. Wind Power Meteorology. Part II: Siting and Models. Wind Energy 1.2: 55-72.

[12] Ayotte, K.W. and Hughes, D.E., 2004. Observations of boundary-layer wind-tunnel flow over isolated ridges of varying steepness and roughness. Boundary-Layer Meteorology 112, 525–556.

[13] Rasouli, A., and Hangan, H., 2013. Microscale Computational Fluid Dynamics Simulation for Wind Mapping Over Complex Topographic Terrains. Journal of Solar Energy Engineering, 135, 041005.

[14] Arya, S.P.S., Capuano, M.E., Fagen, L.C, 1987. Some fluid modeling studies of flow and dispersion over two-dimensional low hills. Atmospheric Environment 21: 753–764.

[15] Kim, H.G., Lee, C.M., Lim, H.C., Kyong, N.H.,1997. An experimental and numerical study on the flow over two-dimensional hills. Journal of Wind Engineering and Industrial Aerodynamics 66: 17–33.

[16] Carpenter, P., Locke, N.,1999. Investigation of wind speeds over multiple two-dimensional hills. Journal of Wind Engineering and Industrial Aerodynamics 83: 109–122

[17] Teunissen, H.W., Shokr M.E., Bowen, A.J., Wood, C.J. and Green, D.W.R., 1987. The Askervein hill project: wind tunnel simulations at three length scales. Boundary Layer Meteorology, 40, 1–29.

[18] Salmon, J. R., Teunissen, H. W., Mickle, R. E., and Taylor, P. A., 1988. The Kettles hill project: field observations, wind-tunnel simulations and numerical model predictions for flow over a low hill. Boundary-Layer Meteorology 43, 309–343

[19] Rasouli, A., and Hangan, H., 2013. Micro-Scale CFD Simulation for Wind Mapping over Complex Topographic Terrains. Journal of Solar (and Wind) Energy Engineering 135–4

[20] McAuliffe B.R. and Larose G.L., 2012. Reynolds-number and surface-modeling sensitivities for experimental simulation of flow over complex topography. Journal of Wind Engineering and Industrial Aerodynamics 104–106: 603–613.

[21] Berg, J., Mann, J., Bechmann, A. Courtney, M.S., and Jørgenson, H.E., 2011. The Bolund experiment, part I: flow over a steep, three-dimensional hill. Boundary-Layer Meteorology, 141:219–243.

[22] Yeow, T.S., Cuerva-Tejero A., and Perez-Alvarez J., 2013. Reproducing the Bolund experiment in wind tunnel, Wind Energy.

[23] Kilpatrick R, Hangan H, Siddiqui K, Parvu D, Lange J, Mann J, Berg J, 2016. Effect of Reynolds number and inflow parameters on mean and turbulent flow over complex topography. Wind Energy Science (Under review)

[24] Hangan, H., 2014. The Wind Engineering Energy and Environment (WindEEE) Dome at Western University, Canada. Wind Engineers, JAWE, 39:4(141).

[25] Manwell, J.F., McGowan J.G., and Rogers A.L., 2009. Wind energy explained, theory design and application, 2nd Ed. Wiley.

[26] Wieringa, J. 1992. Updating the Davenport Roughness Classification. Journal of Wind Engineering and Industrial Aerodynamics, 41-44: 357-368.

[27] Mikkelsen, T, 2014. Lidar-based Research and Innovation at DTU Wind Energy - A Review. Journal of Physics: Conference Series, 524, 012007.

[28] Miller, S. T., Keim, B. D., Talbot, R. W., & Mao, H., 2003. Sea breeze: Structure, forecasting, and impacts. Reviews of Geophysics, 41(3). doi:10.1029/2003rg000124

[29] Kilpatrick, Ryan J., Characterization of Mean and Turbulent Flow over Complex Topography under various Inflow and Geometric Configurations" (2016). Electronic Thesis and Dissertation Repository. 3798.

[30] NBCC, National Building Code User's Guide-Structural Commentaries (Part 4), Canadian Commission on Building and Fire Codes, National Research Council of Canada, Ottawa (2015).

[31] Bitsuamlak, G., T. Stathopoulos, Bedard, C., 2006. Numerical Modeling of Wind Flow Over Different Types of Topography. Wind and Structures, 9, 37-58

[32] Sherry, M., Jacono, D.L., Sheridan, J., 2010. An experimental investigation of the recirculation zone formed downstream of a forward-facing step. Journal of Wind Engineering and Industrial Aerodynamics 98, 888–894.

Chapter 4

4   Conclusions and Future Work

The emergence of wind energy has led to an increased number of wind turbines placed in complex terrain, where predictive models struggle to accurately predict the wind conditions. This study was conducted to investigate the influence of inflow conditions as well as local geometry on the flow over complex terrain. To achieve these goals a full-scale field campaign and scaled physical testing in a laboratory setting were conducted.

Full-scale measurements were undertaken at the Wind Energy Institute of Canada research and development park in Prince Edward Island, Canada. A scanning lidar was deployed to measure the open-water fetch inflow over a steep, sharp-edged escarpment up to the height of a local wind turbine and the near surface flow field up to a height of 20 m. The wind speed measurements were analyzed and the results were presented in the form of velocity and turbulence intensity profiles as well as wake characteristics downstream of the leading edge of the escarpment. A full-scale sea breeze circulatory coastal system was identified in the first half of the measurement period under neutral and stable atmospheric conditions, having large velocity gradients in the lowest heights near the surface with negative shear above a local maximum. In the second half of the measurement period, the inflow was a typical boundary layer was identified under both stable and unstable atmospheric conditions.

The sea breeze inflow had a profound effect on the downstream near surface flow, creating an internal boundary layer with a strong shear layer forming at the edge of the escarpment. The downstream wake decreased with height and the turbulence intensity shows a region near the surface is dominated by geometry while a second peak in turbulence intensity is seen close to the height of the local maximum upstream. Comparatively, under boundary layer conditions, the near surface flow behaviour more closely resembles that of bluff body flow, experiencing a growing wake downstream and a near surface maximum in turbulence intensity which is more influenced by the geometry of the escarpment and extends higher in the vertical direction. The region of reverse flow near the surface is suppressed under sea breeze conditions due to the increased shear in the inflow profile.

To fulfill the second objective, a large-scale model was used to conduct physical testing at the WindEEE dome. The full-scale sea breeze inflow conditions were compared to a typical ESDU open-sea boundary layer profile over three different escarpment geometries from three different wind direction, centered at the location of a local wind turbine. In comparing the sea breeze inflow and the ESDU inflow, the results indicated that the flow was significantly less influenced by the geometry of the escarpment, regardless of direction using a sea breeze inflow compared to a boundary layer inflow. The given fetch of the model and position of the local turbine was not far enough from the coast to experience a developed boundary layer inflow on the new surface under sea breeze conditions, which may cause the turbine roughly 105 m from the coastline to experience negative shear. Full-scale data showed good agreement with the results from the model study under sea breeze inflow conditions, suggesting that the mean flow was simulated well. Moreover, at the wind turbine location, a much better comparison to full-scale data at hub height was achieved using the sea breeze inflow compared to the ESDU inflow conditions, highlighting the abilities of WindEEE to simulate non-ABL flow conditions in coastal regions. The turbulent characteristics of the sea breeze inflow were unrealistic, however, which limited the extent of the flow field study. This was most likely caused by large scale structures shed by the trip feature used to create the inflow profile.

In a detailed comparison of the escarpment geometries using typical boundary layer inflow conditions, the behaviour of the flow field was much different for the three wind directions studies. A small region of reverse flow was observed through flow visualization of a concave section of the escarpment, seen from 230°, which is validated by the turbulent flow characteristics. A turbulent wake formed downstream of the inferred reattachment point, propagating downstream to the turbine location. At a wind direction of 270° the peninsula upstream created a shear layer which effectively created a vertically displaced wake above an accelerated region near the surface creating a speed-up at the wind turbine location. The pointed, upwind sloped escarpment seen form 300° showed very little effect on the flow compared to the other two wind directions suggesting that the local features of the escarpment edge plays a very important role in the downstream flow behaviour.

Through the completion of this study, an increased knowledge of the flow behaviour in complex terrain of unique geometries, in coastal wind conditions has been attained, showing that the flow behavior is significantly altered in thermally driven systems. Additionally, the importance of modelling small scale features, such as upwind and downwind slopes of the escarpment edge are highlights, which can significantly impact the results of a topographical study. Finally, the importance of physically simulating inflow conditions in scaled model testing have proved to be important in accurately representing the flow field for wind resource assessment purposes. The results of the full-scale campaign, and scaled testing also provide data sets for future model comparisons.

5   Future Work

In terms of future work with regards to this study, a secondary field campaign featuring anemometers and directional vanes at multiple locations as well as two more scanning lidars, for a total of three, would allow for a more complete picture of the flow. As the terrain contains many complex features and is subject to sea breezes, it would be interesting to resolve the three-dimensional flow field with three lidars and have a sense of the wind direction further downstream of the escarpment. This would provide a more complete picture for modelers. Additionally, moving the placement of the lidar closer to the wind turbine would allow for a more detailed study of the near surface inflow to the turbine to investigate the effect of the sea breeze inland and potential large scale structures.

Regarding the physical modelling, the biggest issue that must be addressed is the turbulence characteristics of the inflow conditions. Methods that are often used in the wind tunnel, such as mesh screens, may be a viable option for diffusing the large-scale structures that are shed form the trip section used to make the sea breeze inflow. A more advanced technique may be to use the characteristics of the 60-fan wall to pulse an entire row of fans or individual fans to provide more mixing. It would be very interesting to characterize the turbulent statistics and compare them with a typical boundary layer flow. Using Cobra Probes are advantageous compared to a hot-wire, however they are still point measurement techniques and leave a feeling of partial completeness. Using more a

more detailed measurement technique, such as PIV Laser Doppler Velocimetry (LDV), would allow for more of the flow details to be investigate in high quality. This would be especially interesting in the case of the peninsula as snapshot of the flow would provide much more insight into the shear layer present. Additionally, it would be interesting to place a model wind turbine or porous disk at the position of turbine 4 to act as a momentum sink, which would most likely alter the flow characteristics in the upstream vicinity of the wind turbine.

Appendix A: WindScanner Data Analysis Procedure

Synchronization of the wind Doppler Spectra with the corresponding global position is the first step of the data analysis process. This is done by converting motor positions which are recorded by the motor control system into a global coordinate system with the origin at the center of the optical head. For each sample location in space there is a corresponding Doppler spectrum associated with that position. The Doppler spectra are then normalized, or whitened, by a background noise spectrum such that the peaks in the spectrum due to relative intensity noise (RIN) are reduced [1]. The background noise spectrum is generally obtained by measuring the signal obtained while scanning with the optical shutter closed. However, Angelou et al. [1] have found that in some cases scanning with the shutter closed resulted in finding frequencies around the center AOM frequency. This can cause an overestimation in the background noise and reduce the accuracy of the line-of-sight wind speed obtained. Instead, a median value for each frequency bin of the Doppler spectra over a sufficiently long period was taken as the background spectrum. Once the flattened spectrum is obtained, a secondary thresholding method is used to further filter out any remaining structures in the spectrum due to noise. This threshold value determines the limit at which signals above this value are a result of moving aerosols and not noise. Calculation of the threshold value depends on the application of the WindScanner and is different for every experiment, however does have somewhat of a structure when determining its value. The threshold is the mean value plus a somewhat arbitrary number of standard deviations of the Doppler spectrum in a range of frequencies where wind is to be expected. This means that some knowledge of the flow is important in applying a proper threshold value. During the current campaign, reference sensors were set up near the measurement location but not in the immediate area of the WindScanner which were used to determine the local wind conditions. Angleou et al [2] attempted to choose an appropriate threshold value based on the minimum mean difference between consecutive wind speed values which was implemented in the current data analysis. An integer value of the number of standard deviations added to the mean was varied from 0 to 7 with a step size of 0.1. This was

done to obtain the smallest difference between consecutive values to choose an appropriate threshold value. The threshold value chosen was 3.5 standard deviations added to the mean. Finally, an estimate of the Doppler shift frequency was done to obtain a line-of-sight wind speed value. There are three such methods that have been identified [2] each having different characteristics. The first method is defined as the maximum method and the estimated shifted frequency bin is chosen based on the maximum signal in the filtered Doppler spectrum. The second method is based on the location of the median value of the filtered Doppler spectrum which, in this case, can be located between two frequency bins. Finally, the last method uses a centroid function to determine the frequency bin of the Doppler shift. In the case of low turbulence, which can be seen in the Doppler spectra as narrow distinct peaks, the maximum and median method are usually close in the estimation of the Doppler shift frequency bin [2]. In the case of higher turbulence, it is harder to detect which peak the wind signal is as they are shown in the spectra as shorter and wider peaks. For a highly turbulent case the maximum method may be less accurate than the median method. The centroidal method is generally not as accurate as either of the other methods while the median methods is the most robust. An in-house MATLAB code was written based on these principles and the median method was used to determine the Doppler shifted frequency and hence line-of-sight wind speed.

References

[1] Angelou, N., Mann, J., Sjöholm, M., Courtney, M., 2012. Direct measurement of the spectral transfer function of a laser based anemometer. Rev Sci Inst 83(3):33,111

[2] Angelou, N., Foroughi Abari, F., Mann, J., Mikkelsen, T., and Sjöholm, M. Challenges in Noise Removal from Doppler Spectra Acquired by a Continuous-wave Lidar. DTU Orbit.

Curriculum Vitae

Name: Julien LoTufo

Post-secondary Education and Degrees:
Western University
London, Ontario, Canada
2011-2015
Bachelor of Engineering Science
Mechanical and Materials Engineering

The University of Western Ontario
London, Ontario, Canada
2015-Present
Master of Engineering Science
Mechanical and Materials Engineering

Related Work Experience
Teaching Assistant
The University of Western Ontario
2015-Present

Refereed Conference Presentations\Publications:

LoTufo, J., Siddiqui, K., Hangan, H., 2017. Experimental investigation of the influence of inflow conditions on the flow over an extended-edge escarpment. (to appear in) Proceedings of Fluid Engineering Division Summer Meeting (FEDSM). Paper No. FEDSM2017-69534

LoTufo, J., Siddiqui, K., Hangan, H., 2016. Near-surface measurements of flow over an escarpment. CSME International Congress, Kelowna, BC, Canada

LoTufo, J, Parvu, D, Hangan, H., Siddiqui, K., 2015. Shear Layer Effects of Cliff Edges: PEIWEE '15 "WindScanner" Campaign. WindTech 2015: International Conference of Future Technologies in Wind Energy, London, ON, Canada

Non-refereed Conference Presentations\Publications:

LoTufo, J., Siddiqui, K., Hangan, H., 2015. The Use of LiDARs in the Characterization of Flow Fields on Wind Farms. 1000 Islands Energy Research Forum, Alexandria Bay, NY, USA

LoTufo, J., Hangan, H., Siddiqui, K., 2016. Full-scale measurements of the wind field over an escarpment in Prince Edward Island using intrusive and non-intrusive techniques. 1000 Islands Fluid Mechanics Meeting, Gananoque, ON, Canada